Natural Product Reports

ROYAL SOCIETY OF CHEMISTRY

REVIEW

View Article Online
View Journal | View Issue

Cite this: *Nat. Prod. Rep.*, 2026, **43**, 746

Structure, bioactivity, biosynthesis, and synthesis of corynanthe alkaloids

Chenxu Liu,[a] Mengqi Tong,†[a] Kouharu Otsuki,[b] Wei Li,[b] Feng Feng*[a] and Jie Zhang*[a]

Covering: 2006–2025

Corynanthe alkaloids constitute the largest class of monoterpene indole alkaloids and feature a secologanin-derived carbon skeleton fused to an indole or indole-derived heterocycle. To date, thousands of structurally diverse members have been identified, exhibiting activities ranging from anti-inflammatory and antihypertensive to neuroprotective effects. Growing insight into ajmaline biosynthesis and recent advances in the synthetic construction of corynantheine-type scaffolds have renewed interest in this family. However, contemporary reviews largely emphasize structural diversity and biological function, while offering limited systematic coverage of biosynthetic logic or total-synthesis strategies. The present review compiles corynanthe alkaloids reported between 2006 and 2025 and summarizes their natural sources. It also provides an integrated overview of recent progress in both biosynthetic elucidation and chemical synthesis of simple corynanthe alkaloids and yohimbine alkaloids, alongside a concise survey of their biological activities. Collectively, this review aims to stimulate new perspectives on the discovery and synthetic innovation of corynanthe alkaloids, providing a valuable resource for researchers in natural-product chemistry and drug development.

Received 12th July 2025

DOI: 10.1039/d5np00051c

rsc.li/npr

[a]*School of Traditional Chinese Pharmacy, China Pharmaceutical University, Nanjing 211198, China. E-mail: 1020152495@cpu.edu.cn; fengfeng@cpu.edu.cn; Tel: +86 25-86185418*

[b]*Faculty of Pharmaceutical Sciences, Toho University, Miyama 2-2-1, Funabashi, Chiba 274-8510, Japan*

† Equal contribution authors.

1 Introduction

Plants generate a diverse range of organic compounds through secondary metabolic processes.[1] Alkaloids are plant-produced specialized metabolites with nitrogen atoms from amino acids incorporated into heterocyclic structures. A specific group of these alkaloids, known as monoterpene indole alkaloids (MIAs), is classified based on the biosynthetic origin.[2] MIAs constitute one of the most structurally diverse alkaloid groups, with over 2500 distinct molecules identified to date. These compounds are predominantly found in the plant families such as Apocynaceae, Loganiaceae, and Rubiaceae.[2–4] While the functions of many MIAs remain largely unexplored, recent studies have demonstrated their capacity to confer protection to host plants against specific herbivores.[5] Corynanthe alkaloids represent a class of tetracyclic monoterpene natural products characterized by an intact secologanin carbon skeleton fused to an indole or indole-derived heterocyclic.[6] The unique architecture of corynanthe alkaloids serves as a biosynthetic precursor for numerous MIAs, highlighting their central role in MIA research. The corynanthe alkaloids also include yohimbine-type alkaloids, oxindole corynanthe-type alkaloids, mavacurane-type alkaloids, sarpagine-type alkaloids, akuammiline-type alkaloids, and ajmaline-type alkaloids.[7]

In 2019, eight prestigious laboratories renowned for their contributions to the field of MIA chemistry established a tandem mass spectrometry (MS/MS) knowledge base specializing in this class of natural products (NPs) and named it the Monoterpene Indole Alkaloids DataBase (MIADB).[8] By 2025, the MIADB had 422 MS/MS spectra with full structural annotations and 80 skeletons. Beniddir *et al.*[9] proposed a "spectral skeleton" correlation strategy that used Tanimoto structural similarity analysis and improved cosine similarity scoring to reveal the highly conserved mass spectral behavior of ajmalicine and corynantheane spirooxindoles. As a key scaffold among MIAs, corynanthe alkaloids clearly demonstrate their significant research value. Using the SpectraToQueries tool, specific fragmentation patterns of the corynanthe spirooxindole subtype were successfully extracted, enabling the construction of highly efficient MassQL queries.[10–12] During the screening of 75 plant extracts, the method successfully identified multiple corynanthe-type compounds with an accuracy rate of 55.56%, significantly improving the identification efficiency of such compounds in complex mixtures. This achievement not only provides a reliable tool for the high-throughput discovery and structural identification of corynanthe alkaloids, but also establishes a solid foundation for subsequent activity screening and functional studies.

The unique chemical structure of corynanthe alkaloids determines diverse biological activities, which have attracted great interest from researchers. Notably, the enhancement of MIADB furnishes powerful data mining capabilities and novel strategies for structural characterization in the research on corynanthe alkaloids and natural products. Recent studies on corynanthe alkaloids have achieved significant progress in biosynthetic research, particularly in elucidating key enzymes and metabolic pathways. Heterologous biosynthesis using engineered yeast and *Nicotiana benthamiana* has emerged as a prominent strategy for scalable production. In chemical synthesis, structural complexity has been addressed through bio-inspired strategies and novel catalytic approaches. Meanwhile, modular synthetic frameworks and retrobiosynthetic methodologies have streamlined synthetic routes, thereby substantially improving efficiency and stereochemical precision. Although several studies have been conducted on these compounds, a comprehensive systematic review that integrates their biosynthesis and chemical synthesis remains conspicuously lacking. In this paper, we present a detailed review of recent advances in the structural characterization, biosynthetic pathway, total synthesis, and biological activity of corynanthe alkaloids, thereby contributing to future research and potential applications in this field.

2 Structure

Corynanthe alkaloids are primarily isolated from *Mitragyna speciosa* (commonly known as kratom) and *Corynanthe pachyceras* K. Schum.[13] Notably, compounds such as mitragynine (**1**), corynantheidine (**2**), corynantheine (**3**) (Fig. 1). Mitragynine (**1**) exhibits potent G-protein-selective agonistic activity at μ-opioid receptors (MORs).[14–16] But unlike classical MOR agonists, it may be associated with minimal adverse side effects.[6] The fundamental structure of MIAs is composed of tryptamines and monoterpenes or their derivatives, monoterpene rearrangements of corynanthe alkaloids lead to their structural and chemical diversity.[7]

Geissoschizine (**4**) was isolated from *Catharanthus roseus* and *Rhazya stricta*.[17–19] As a key intermediate in the biosynthesis of MIAs, it plays a central role *in vivo* synthesis of nearly all MIAs. Moreover, it has been shown that the *E*-configuration of geissoschizine's C19–C20 double bond promotes secondary cyclization by stabilizing the *cis*-quinolizidine conformation, whereas the *Z*-configuration induces a *trans*-quinolizidine conformation that sterically obstructs the reaction.[20] Tetrahydroalstonine (**5**) isolated among others from *Alstonia scholaris*,[21] *R. stricta*,[22] *Ophiorrhiza discolor*,[23] and *C. roseus*[20] with high purity and demonstrated the neuroprotective effect of tetrahydroalstonine (**5**) against OGD/R-induced neuronal damage in cortical neurons. Hirsutine (HSN) (**6**) exhibits a broad range of pharmacological properties, including antihypertensive, antiarrhythmic, cardioprotective, and antimetastatic effects. These properties are attributed to its ability to inhibit calcium ion (Ca^{2+}) influx and modulate intracellular Ca^{2+} release.[24–26] Ajmalicine (**7**) is a natural alkaloid primarily isolated among others from *Rauvolfia serpentina*,[27] *C. roseus*,[18] and *M. speciosa*.[21,28] Xiao *et al.*[29] isolated yohimbine (**8**) from *Pausinystalia yohimba*, which has been traditionally utilized as a stimulant and aphrodisiac. Furthermore, yohimbine (**8**) has been demonstrated to exhibit antidiuretic, antiadrenergic, and serotonin-antagonist properties. Rauwolscine (**9**) possesses diverse biological activities, including α_2-adrenergic receptor antagonism and antihypertensive effects.[30] Reserpine (**11**), derived from *R. serpentina*, is an effective antihypertensive drug.

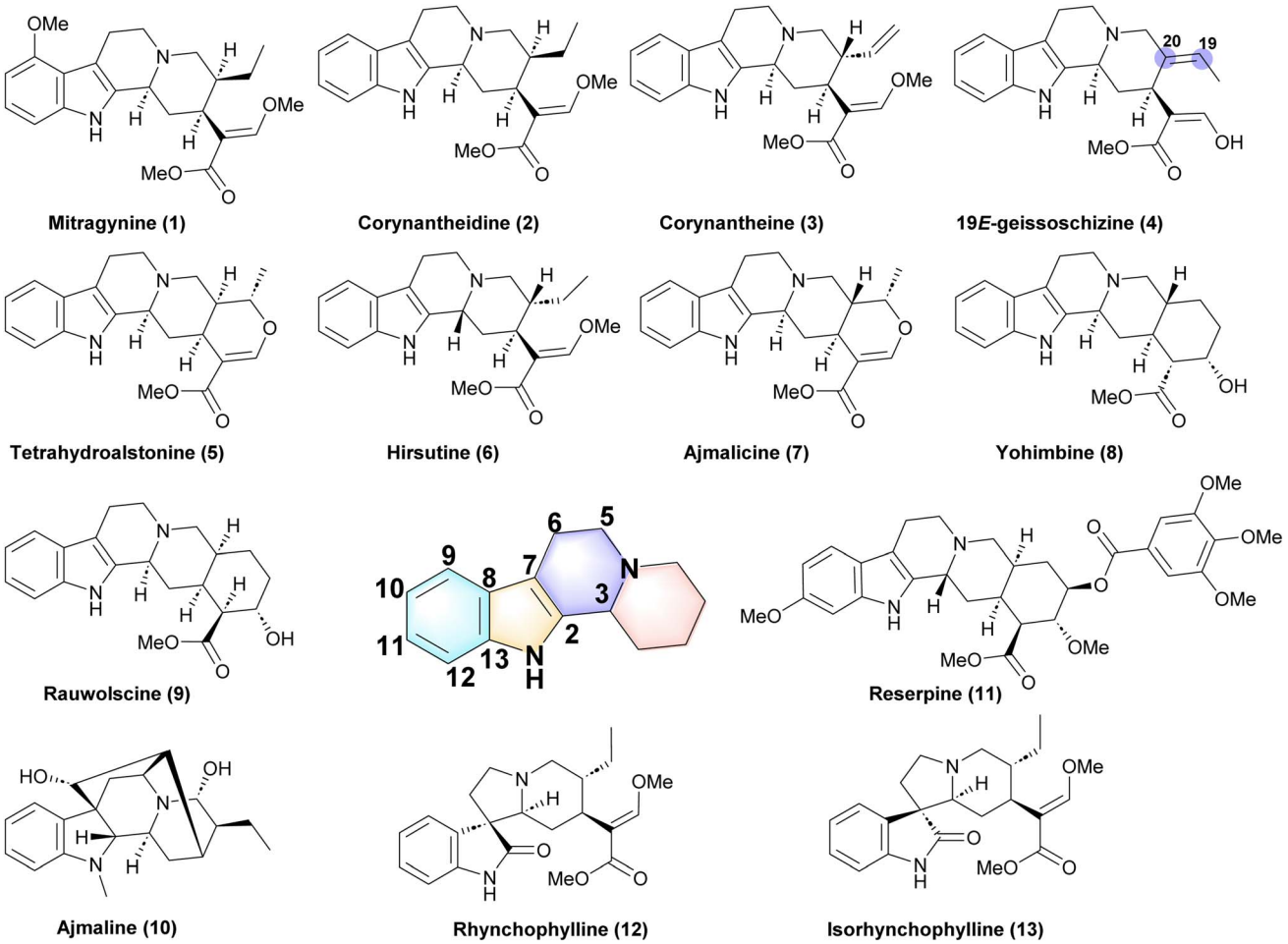

Fig. 1 The skeleton structure of corynanthe alkaloids and related compounds.

However, its clinical use has declined due to its potential to cause depression.[31] Ajmaline (**10**), a potent antiarrhythmic agent, functions as a sodium channel blocker and is widely used as a diagnostic pharmacological tool for identifying brugada syndrome (a disorder associated with an increased risk of life-threatening arrhythmias and sudden cardiac death).[32] Rhynchophylline (**12**) and isorhynchophylline (**13**), primarily derived from *Uncaria rhynchophylla*, exhibit neuroprotective, antihypertensive, and anti-inflammatory activities.[33,34]

Nauclorienine (**14**) were simple corynanthe-type alkaloids isolated from the 90% EtOH extract of the stems and leaves of *Nauclea orientalis* (Fig. 2) and (Table 1).[35] Subditine (**15**) were isolated from the bark of *Nauclea subdita*.[36] Yu *et al.*[37] isolated nine new corynanthe-type alkaloids (**16–24**) from the seeds of *Strychnos angustiflora*. The structure of **16** was confirmed using single-crystal X-ray crystallography. Based on the nuclear magnetic resonance spectroscopy (NMR) and electronic circular dichroism (ECD), the *R*-configuration of the *N*-4 stereogenic center of **17** was shown to be opposite to the **16**. The identification of the compounds **18–23** extends the range of analogues of this group of natural products containing the chain possessing syringoyl moiety and glucose in corynanthe-type alkaloid. Compounds **25–28** were isolated from *A. scholaris*.[38] Epicatechocorynantheines A (**29**) and B (**30**), and epicatechocorynantheidine (**31**) were isolated from the stem bark of *C. pachyceras*.[2] These compounds represent the examples of corynanthean-type alkaloids tethered with a flavonoid. Compound **31** notably instigated two connections between the MIA and the flavonoid, yielding an unprecedented octacyclic appendage.

Hunterizeylines H (**32**) were isolated from an aqueous MeOH extract of the twigs and leaves of *Hunteria zeylanica* (Fig. 3).[39] Compounds **33–37** represent the examples of heterodimeric frameworks composed of a gelsedine-type alkaloid and a modified corynanthe-type. They were isolated from the fruits of *Gelsemium elegans*.[40] Compounds **38–42** were isolated from the trunk bark of *Tabernaemontana penduliflora* K. Schum. These compounds were recovered as an inseparable mixture of isomeric pairs that differ only in the orientation of the *N*-methyl group.[41] Rauvomitorine I (**43**), rauvines A (**44**) and B (**45**) were obtained from the leaves of *Rauvolffa vomitoria* Wennberg.[42,43] Compounds **46–48** were isolated from the stems of *Uncaria hirsuta* Havil, which are oxidindole alkaloids and contain an oxindole moiety (N–C=O) in ring B.[44] Rhynchophylloside F (**49**), an oxindole alkaloid characterized by a seven-membered D-ring configuration, was isolated along with structurally related

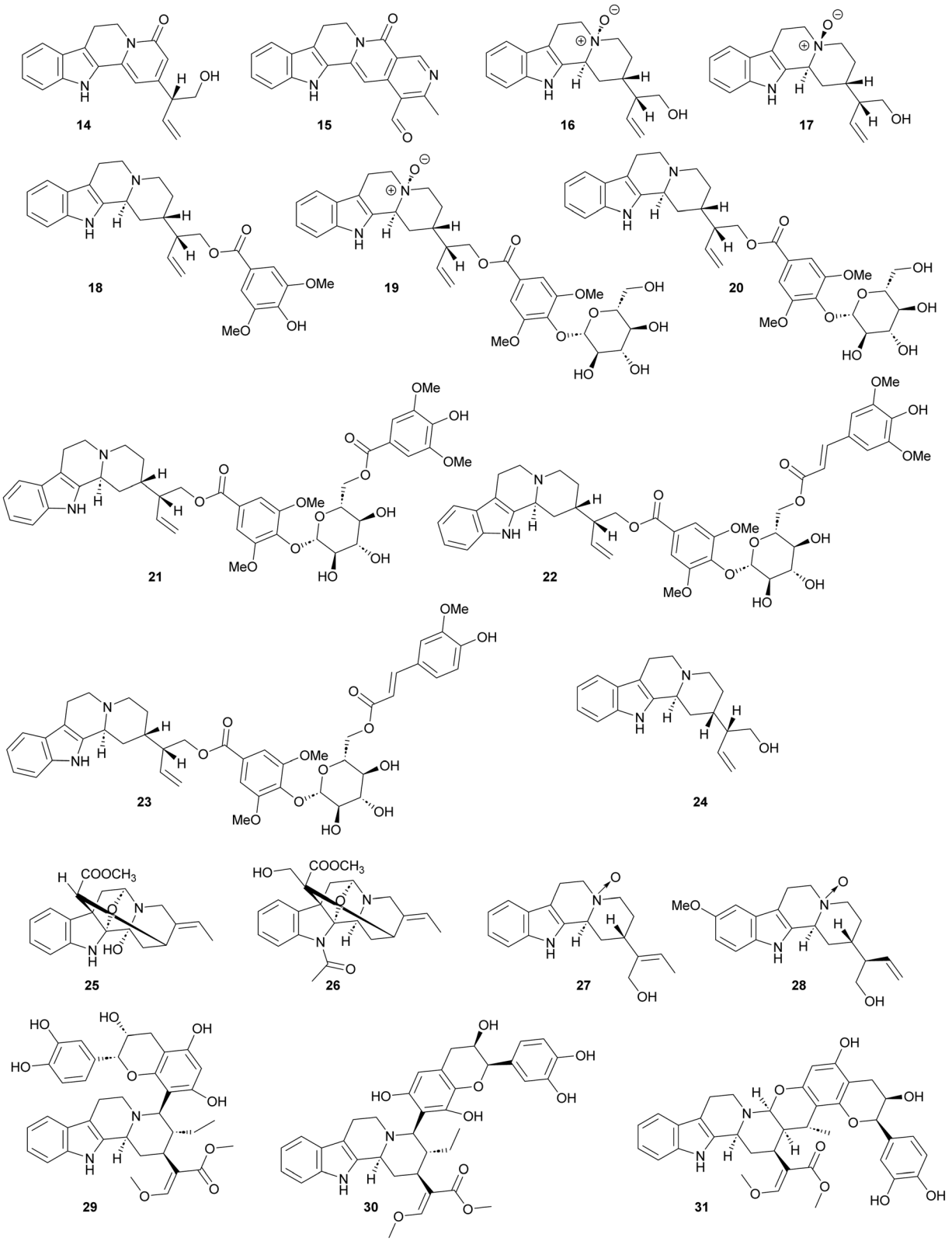

Fig. 2 The structure of compounds **14–31**.

analogues **50–53** from the medicinal plant *U. rhynchophylla* (Miq.) Miq. ex Havil.[45]

7-Hydroxypleiocarpamine (**54**) and 6-oxopleiocarpamine (**55**) were isolated from the bark and leaf extracts of *Alstonia angustifolia*. 7-Hydroxypleiocarpamine (**54**) has two possible structures to be considered, which differ only in the configuration at C-7.[46] The N_4-lactam in normavacurin-21-one (**56**) contains a carbonyl group linked to C19–C20-ethylidene.[47]

Table 1 Corynanthe alkaloids (compounds **14–68**) isolated between 2006–2025 and their sources

No.	Compound name	Plant part	Source	References
14	Naclorienine	Stems and leaves	*Nauclea orientalis*	35
15	Subditine			
16	(3*S*,4*S*,15*S*,20*R*)-Antirhine N_4-oxide	Seeds	*Strychnos angustiflora*	37
17	(3*S*,4*R*,15*S*,20*R*)-Antirhine N_4-oxide			
18	21-*O*-Syringoylantirhine			
19	21-*O*-Syringoyl-(3*S*,4*S*,15*S*,20*R*)-antirhine N_4-oxide 4′-*O*-β-*d*-glucopyranoside			
20	21-*O*-Syringoylantirhine 4′-*O*-β-*d*-glucopyranoside			
21	21-*O*-Syringoylantirhine 4′-*O*-[6″-*O*-syringoyl]-β-*d*-glucopyranoside			
22	21-*O*-Syringoylantirhine 4′-*O*-[(*E*)-6″-*O*-sinapoyl]-β-*d*-glucopyranoside			
23	21-*O*-Syringoylantirhine 4′-*O*-[(*E*)-6″-*O*-feruloyl]-β-*d*-glucopyranoside			
24	Antirhine			
25	Meloslines C	Roots	*Alstonia scholaris*	38
26	Meloslines D			
27	Meloslines E			
28	Meloslines F			
29	Epicatechocorynantheines A	Stem bark	*Corynanthe pachyceras*	2
30	Epicatechocorynantheines B			
31	Epicatechocorynantheidine			
32	Hunterizeylines H	Twigs and leaves	*Hunteria zeylanica*	39
33	Gelsecorydines A	Fruits	*Gelsemium elegans*	40
34	Gelsecorydines B			
35	Gelsecorydines C			
36	Gelsecorydines D			
37	Gelsecorydines E			
38	Penduflorines A	Trunk bark	*Tabernaemontana penduliflora* K. Schum	41
39	Penduflorines B			
40	Penduflorines C			
41	Penduflorines D			
42	Penduflorines E			
43	Rauvomitorine I	Leaves	*Rauvolfia vomitoria* Afzel	42 and 43
44	Rauvines A			
45	Rauvines B			
46	Hirsutanine D	Stems	*Uncaria hirsuta* Havil	44
47	Hirsutanine E			
48	Uncarine B *N*-oxide			
49	Rhynchophyllosides F	Stems	*Uncaria rhynchophylla* Miq. ex Havil	45
50	Rhynchophyllosides G			
51	Rhynchophyllosides H			
52	Rhynchophyllosides I			
53	Rhynchophyllosides J			
54	7-Hydroxypleiocarpamine	Bark and leaves	*Alstonia angustifolia* Wall. ex A. DC	46
55	6-Oxopleiocarpamine			
56	Normavacurine-21-one	Leaves	*Alstonia scholaris* (L.) R. Br	47
57	Hunterizeyline F	Twigs and leaves	*Hunteria zeylanica* Gardner ex Thwaites	39
58	22-Demethyl MMV	Bark	*Tabernaemontana macrocarpa* Jack	48
59	22-Deethyl fuchsiaefoline			
60	N_4-methyltalpinine	Stem bark	*Alstonia angustifolia* Wall. ex A. DC	49
61	*O*-Acetyltalpinine	Leaves and stem bark	*Alstonia angustifolia* Wall. ex A. DC	46
62	Talpinine			
63	Alstopenidine H	Leaves and stem bark	*Alstonia penangiana* Sidiy	50
64	Vincamaginine A	Leaves	*Malayan Alstonia penangiana*	51
65	Vincamaginine B			
66	Nicalaterine A	Bark	*Hunteria zeylanica* (Retz.) Gardner ex Thwaites	52
67	Cathafoline	Bark	*Tabernaemontana dichotoma* Roxb	53
68	Kopsiyunnanine B	Aerial	Yunnan *Kopsia arborea*	54

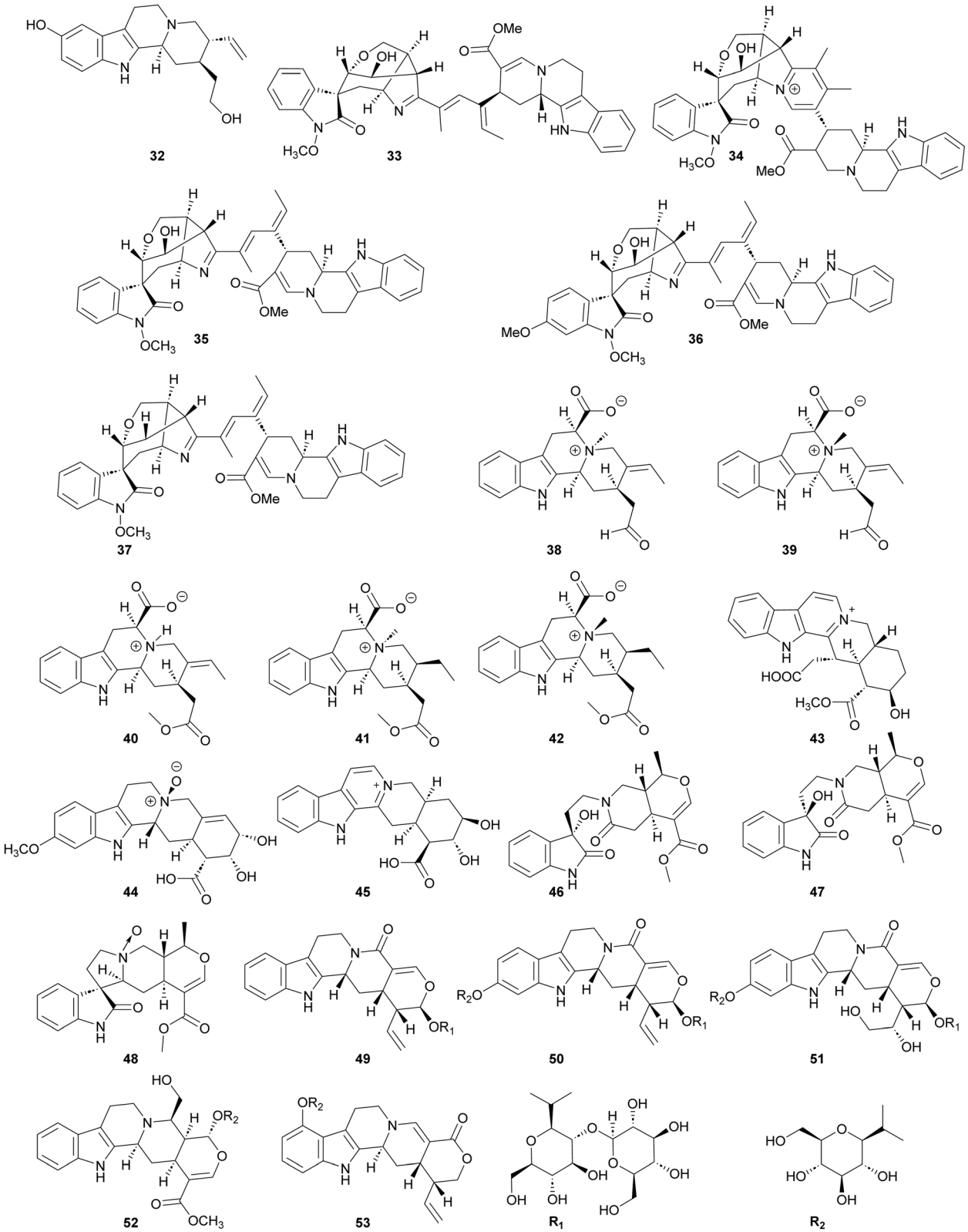

Fig. 3 The structure of compounds 32–53.

Hunterizeyline F (**57**) is a sarpagane-mavacurane bisindole alkaloid.[39] Quaternary ammonium alkaloids **58** and **59** were found in the bark of *Tabernaemontana macrocarpa* Jack.[48] *N*(4)-methyltalpinine (**60**) has a carbinolamine group, which was isolated from the stem bark of *Alstonia angustifolia*.[49] *O*-Acetyltalpinine (**61**) is the *O*-acetyl derivative of talpinine (**62**).[46]

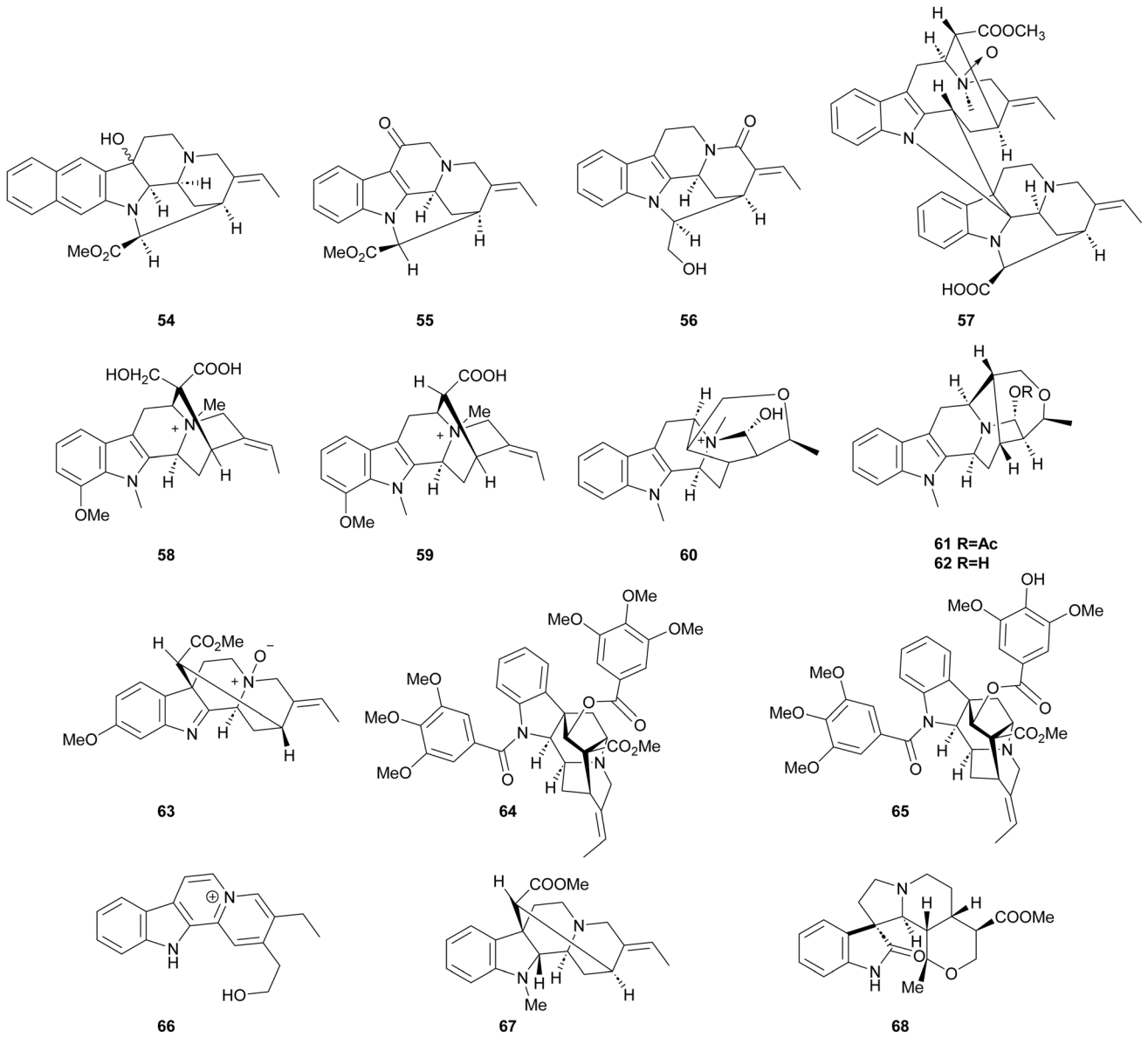

Fig. 4 The structure of compounds **54–68**.

Alstopenidine H (**63**) is the *N*-oxide of 11-methoxystrictamine.[48] Compounds **64** and **65** were isolated from the EtOH extract of *Malayan Alstonia penangiana* Sidiy.[51] Nicalaterine A (**66**) was isolated from the *Hunteria zeylanica* (Retz.) Gardner ex Thwaites bark.[52] Cathafoline (**67**) was isolated from *Tabernaemontana dichotoma* Roxb.[53] Kopsiyunnanine B (**68**) is a corynanthe oxindole alkaloid rotated by the D ring (Fig. 4).[54]

3 Biosynthesis

In contrast to prokaryotes, genes encoding metabolic pathways in plants are not typically clustered together. Consequently, the identification, cloning, and isolation of each enzyme in the synthetic pathway are necessary, which presents a significant challenge to the complete elucidation of alkaloid biosynthesis.[55] Corynanthe alkaloids are biosynthesized through the condensation of tryptamine derivatives with cyclic enol ether terpenoids and enzymatic modifications (*e.g.*, strictosidine synthase (STR), strictosidine β-*d*-glucosidase (SGD)), which lead to the formation of structurally diverse and complex alkaloid derivatives. These transformations are catalyzed by specific enzymes that mediate key biochemical processes, including selective C–C bond cleavage and oxidative rearrangement reactions, which collectively contribute to the structural diversification of the alkaloid scaffold.[56] Courdavault *et al.*[57] combined spatial transcriptomics and MYC2 (a transcription factor in the jasmonate signaling pathway) overexpression in *A. scholaris* to identify a multifunctional geissoschizine cyclase (GC2) that catalyzes C–C and C–N bond formations, yielding akuammicine, strictamine, and 16-*epi*-pleiocarpamine. Though progress has been made in identifying the biosynthetic genes for catharanthine and vindoline in *Rosa* spp. through forward

genetics, gaps still exist in our understanding of the complete enzymatic repertoire. Homology-based cloning helps identify pathway enzymes like acyltransferases and cytochrome P450s (CYP450), but it requires extensive functional validation and is limited by the availability of substrates for enzyme reactions.[58]

3.1 Biosynthesis pathway of strictosidine

Isopentenyl diphosphate (IPP, **69**) and dimethylallyl diphosphate (DMAPP, **70**) are the primary precursors of terpenoid alkaloids and give rise to iridodial,[59] which is subsequently converted into loganic acid through the sequential activities of iridodial oxidase (IO), 7-deoxyloganetic acid glucosyltransferase (7-DLGT), 7-deoxyloganic acid hydroxylase (7-DLH), and loganic acid methyltransferase (LAMT). Secologanin synthase (SLS) then catalyzes the oxidative ring opening of loganin to yield secologanin (77), the final terpene precursor required for MIA biosynthesis.[60] Most MIAs originate from the common intermediate strictosidine (**80**) (Scheme 1).[61,62]

3.2 STR/SGD enzymatic specificity and its biosynthetic implications

Strictosidine (**80**) functions as a universal biosynthetic precursor for an exceptionally diverse array of indole alkaloids, including ajmaline-, corynanthe-, aspidosperma-, quinoline-, and iboga-type scaffolds. Its high biochemical plasticity enables species-specific enzymatic tailoring, positioning strictosidine (**80**) as the central molecular hub for MIA diversification.[63] Approximately 2000 known indole alkaloids arise from strictosidine (**80**).[64,65] The strictosidine aglycone can also undergo spontaneous rearrangements to produce 4,21-dehydrogeissoschizine (**81**), which is subsequently reduced by dedicated alcohol dehydrogenases (ADHs). These reduced intermediates feed into multiple specialized metabolic branches that generate the extensive structural diversity observed among downstream MIAs, underscoring the pivotal contribution of ADHs to MIA biosynthetic complexity.[66] STR was first cloned from *R.*

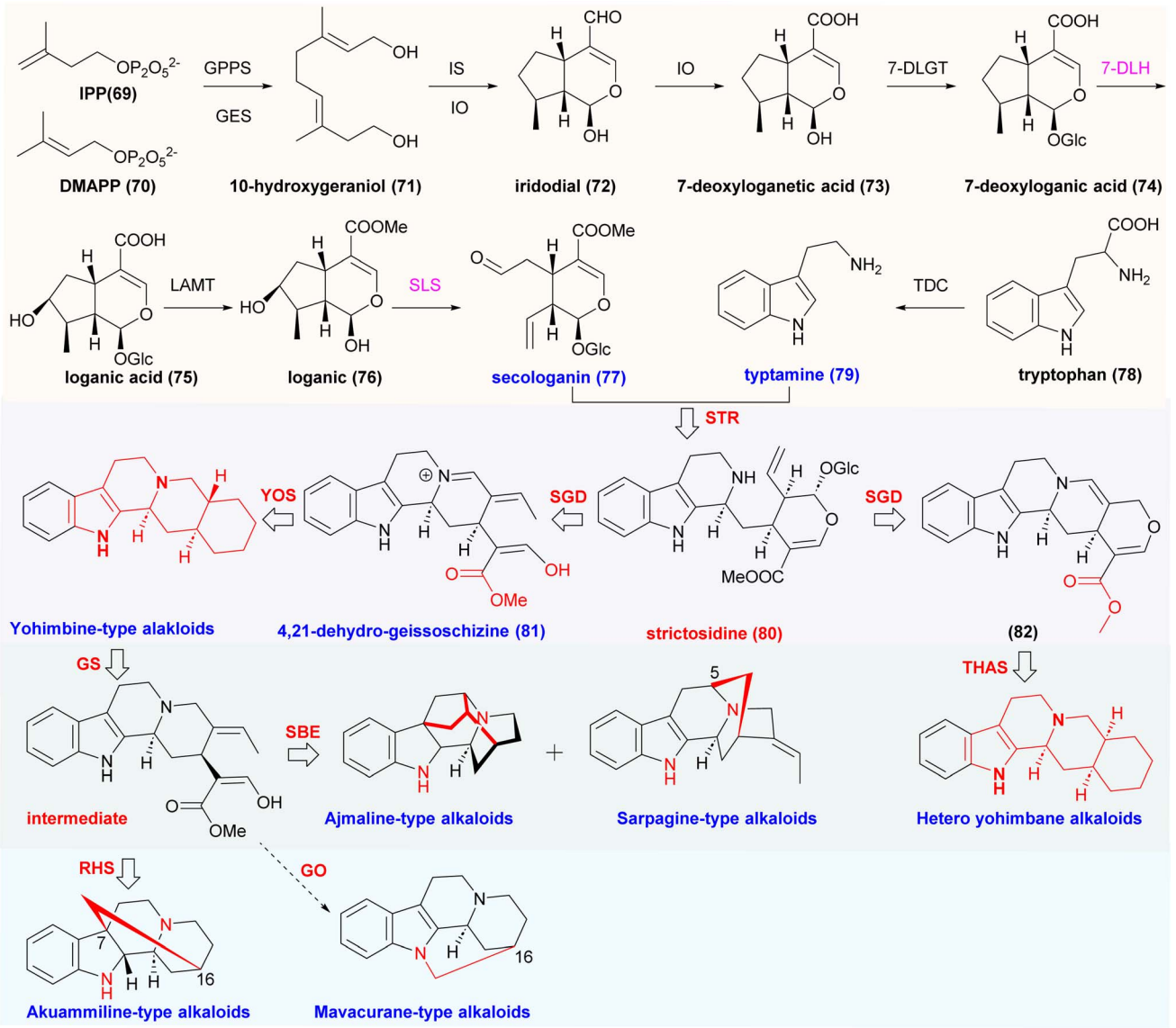

Scheme 1 Biosynthetic pathway for STR and different corynanthe alkaloids.

serpentina and functionally expressed in *Escherichia Coli*,[67] and homologous STRs have since been identified in *C. roseus* and *Ophiorrhiza Pumila*.[68–70]

STR and SGD form the core enzymatic module governing MIA biosynthesis. STR stereospecifically catalyzes the Pictet–Spengler (P–S) condensation between tryptamine (**79**) and secologanin (77) to produce strictosidine (**80**) (Scheme 1).[71–73] The catalytic residue Glu309 (E309) plays a decisive role in substrate recognition; Lin *et al.*[74] showed that steric constraints prevent *N*-methylated tryptamines from properly aligning with E309, SGD then catalyzes the deglycosylation of strictosidine (**80**), exhibiting strictosidine-specific activity with micromolar-range K_m values and functioning as a 63 kDa oligomeric complex.[75] The liberated aglycone rearranges spontaneously into 4,21-dehydrogeissoschizoschizine (**81**), which is subsequently reduced by ADHs to direct metabolic flux toward three major MIA lineages: corynanthe-, iboga-, and aspidosperma-type alkaloids.[66,76] Recent co-expression analyses identified STR isoforms (UrSTR1/5) co-regulated with other MIA pathway genes, and highlighted conserved catalytic residues (UrSTR1: Glu309, Tyr155; UrSTR5: Glu295, Tyr141) essential for strictosidine (**80**) formation.[77] These mechanistic insights not only clarify the enzymatic basis of MIA diversification but also enable metabolic engineering applications, including the heterologous biosynthesis of rhynchophylline (**12**).[74] The stringent substrate selectivity of STR and SGD ensures precise control of MIA biosynthetic flux, making them indispensable targets for synthetic biology strategies aimed at producing rate or non-natural alkaloid derivatives.[78] Consequently, enhancing STR gene expression is a key strategy for improving yields of MIAs that are difficult to obtain. Understanding the regulatory and biochemical factors that influencing STR expression provides critical insight into the entire biosynthesis pathway of strictosidine (**80**) biosynthesis and helps in gaining an in-depth understanding of plant metabolism.[79]

3.3 The role of CYP450 in biosynthesis

CYP450 enzymes play central roles in MIA biosynthesis due to their catalytic versatility in oxidative transformation.[80] Specific CYP450 subfamilies—including CYP71, CYP72, CYP76, and CYP82—mediate distinct steps and exhibit notable substrate specificity.[81] The CYP72 and CYP76 families are essential for secologanin (77) formation through the cycloalkenyl ether ketone pathway,[82] whereas CYP71 and CYP82 enzymes oxidize a broad range of MIA scaffolds (Scheme 2).[83] Secologanin (77), a secoiridoid monoterpene, is produced from loganin *via* SLS (EC 1.14.19.62), a P450 enzyme operating in the mevalonate pathway.[84] The CYP71 family is a major driver of MIA diversification, transforming simple seco- and hetero-yohimbine intermediates into sarpagan,[85] strychnos,[86–88] akuammilan,[88] iboga,[89] and aspidosperma-type alkaoloids.[90,91]

In ajmaline biosynthesis, CYP450 monooxygenases such as the sarpagan bridge enzyme catalyze the oxidative cyclization of 19*E*-geissoschizine (**4**) to polyneuridine aldehyde, while vinorine hydroxylase (VH; CYP82 family) mediates converts vinorine to vomilenine (**87**).[85,92–94] CYP450-mediated oxidations are also critical for ajmalicine (7) formation through the stereospecific

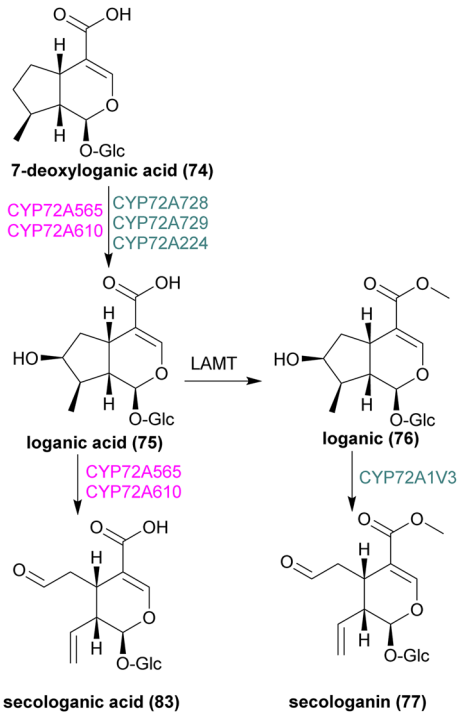

Scheme 2 CYP family enzymes involved in MIA biosynthesis.

hydroxylation of tetrahydroalstonine (**5**).[95,96] Recent work in *U. rhynchophylla* identified CYP450s and flavin-containing monooxygenases (FMOs) potentially involved in the biosynthesis of rhynchophylline (**12**) and isorhynchophylline (**13**), underscoring their importance in spiroindole alkaloid formation.[74,97] Jiang *et al.*[98] characterized two CYP450 enzymes involved in rauwolscine (**9**) biosynthesis and elucidated the pathway leading to reserpine (**11**). Dang *et al.*[99] identified a kratom-derived CYP450 responsible for generating 3-*epi*-corynoxeine (3*R*,7*R*) and isocorynoxeine (3*S*,7*S*) from (3*R*)-secoyohimbane precursors. O'Connor and colleagues[100] characterized three CYP450 enzymes in *C. roseus*—CrGO, CrRS, and CrSBE—that divert geissoschizine into strychnos-, akuammiline-, sarpagan-, and mavacurane-type scaffolds. Notably, CrGO also catalyzes a minor C16–N1 coupling to form mavacurane alkaloids, a function supported by gene-silencing studies. This enzyme, when expressed in *Saccharomyces cerevisiae*, enables efficient *in vivo* and *in vitro* production of spirooxindoles. Collectively, the remarkable substrate specificity and catalytic flexibility of CYP450s provide fine-grained control over corynanthe alkaloid biosynthesis, making them indispensable for natural product diversification and metabolic engineering of bioactive corynanthe derivatives.

3.4 The biosynthesis of representative corynanthe alkaloids

The limited natural availability of MIAs further emphasizes the need for alternative production platforms; for instance, obtaining just 1 g of vincristine requires approximately 2000 kg of dried leaves.[101–103] Alongside the intrinsic synthetic challenges posed by their structural complexity and high stereochemical density, these limitations have driven the

development of heterologous biosynthetic systems.[104,105] Advances in metabolic engineering now allow partial and complete reconstruction of MIA pathways in microbial hosts, offering scalable and sustainable production routes.[106]

In 2016, the γ-tocopherol-like *N*-methyltransferase family was identified as responsible for indole and side-chain *N*-methylation in ajmaline (**10**) biosynthesis.[107] By 2024, the full ajmaline pathway had been elucidated and functionally reconstituted in *S. cerevisiae*. Key reductases—vomilenine 1,2(*R*)-reductase (VR), 1,2-dihydrovomilenine 19,20(*S*)-reductase (DHVR), and 17-*O*-acetylnorajmaline acetylesterase (AAE)—were dentified as essential for vomilenine (**87**) reduction and subsequent acetylation (Scheme 3).[108] Their characterization suggests that vomilenine (**87**) is first reduced by VR, and then further reduced by DHVR to form 17-*O*-acetylnorajmaline (**89**). VR accepts only vomilenine as the substrate but not 19,20-dihydrovomilenine. Although DHVR also exhibits the 19,20-reductase activity of vomilenine (**87**), it shows a 34-fold higher affinity for 1,2(*R*)-dihydrovomilenine (**88**) than for vomilenine (**87**). Supplementing yeast cultures with 5 mg L^{-1} (14.5 μM) of vomilenine (**87**) resulted in titers of 46 μg L^{-1} ajmaline (**10**), demonstrating that high intracellular levels of vomilenine (**87**) are required for efficient downstream flux. Increasing the copy number of VR and tDHVR further enhanced ajmaline (**10**) production twofold (96–128 μg L^{-1}), confirming that VR and DHVR constitute rate-limiting steps in yeast-based biosynthesis of ajmaline (**10**). Despite achieving the *de novo* biosynthesis of ajmaline (**10**), the overall yield remains low due to the instability of key intermediates—including polyneuridine aldehyde and 16-*epi*-vellosimine—and incomplete understanding of VR and DHVR catalytic mechanisms, particularly regarding stereoselectivity and active-site architecture. A high-quality genome assembly is needed to identify AAE and DHVR variants and resolve sequence inconsistencies that may arise from gene duplication or differential expression.

The first heteroyohimbine synthase (HYS) was attributed to O'Connor's group in 2006. A decade later, in 2016, a cluster of homologous HYS enzymes sharing ~96% sequence identity was identified, one of which generated a pair of diastereomers.[109] Notably, a single HYS enzyme can produce multiple isoyohimbine alkaloids, although the underlying determinants of this stereochemical flexibility remain unresolved. Advances in 2023 using multi-omics approaches revealed that yohimbine-alkaloid biosynthesis additionally involves medium-chain dehydrogenase/reductase and tetrahydroalstonine synthase (THAS), both yielding diastereomeric mixtures (Scheme 4).[110] Crystal structures of—THAS1, THAS2, and HYS—uncovered key architectural features governing stereoselectivity. In particular, the active-site configuration—especially the flexible loop 2 region—emerged as a major determinant. HYS, possesses an extended loop 2 that positions a histidine residue (His127) to protonate the substrate from the opposite face, thereby enabling formation of *R*-configured ajmalicine (7).[109,110] Subcellular localization also plays a regulatory role. While SGD resides in the nucleus, downstream enzymes such as RtTHAS3 lack nuclear localization signals. This spatial separation constrains access to the reactive aglycone intermediate and modulates metabolic flux, consistent with the limited in plant activity of RtTHAS3. Despite recent progress, many predicted gene functions remain experimentally unverified, and the catalytic mechanisms underlying the formation of yohimbane isomers—including rauwolscine (**9**) and yohimbine (**8**)—require further elucidation.

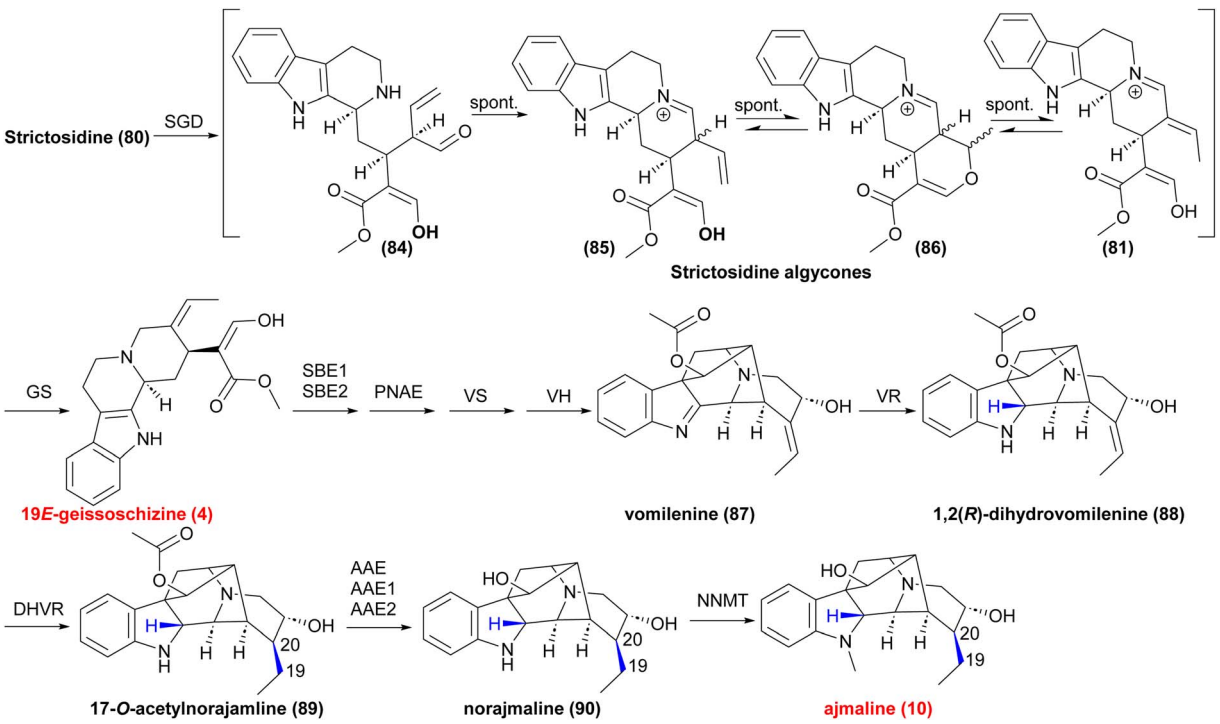

Scheme 3 The biosynthesis of ajmaline by Qu's group.[108]

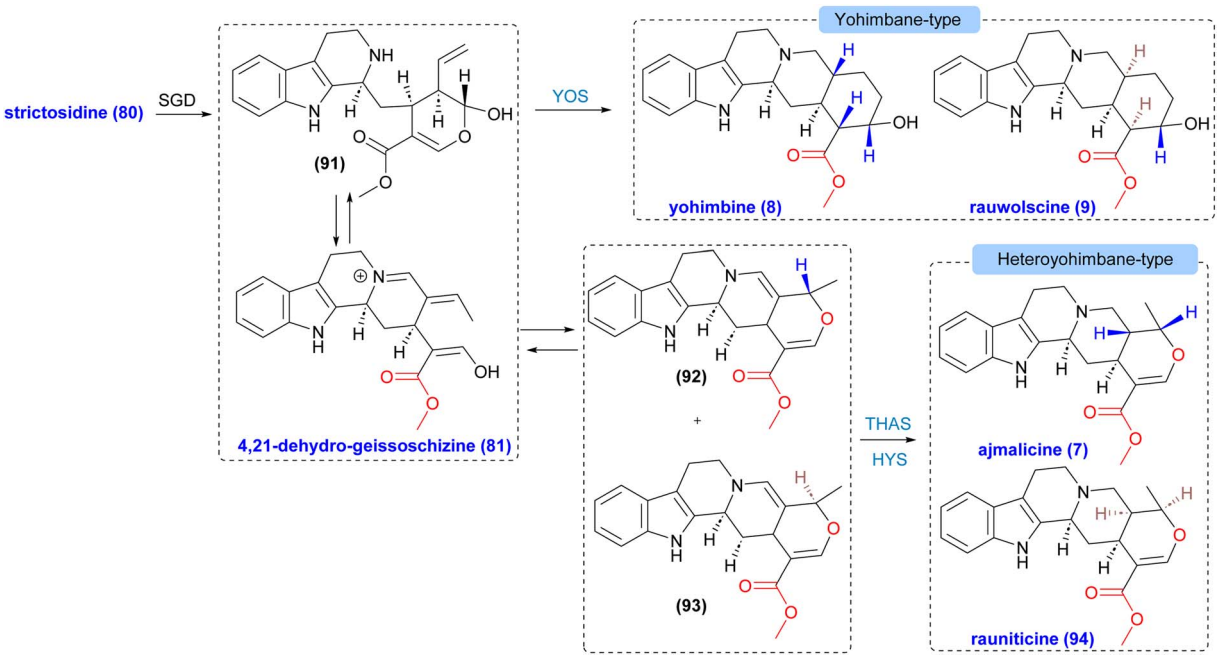

Scheme 4 O'Connor's proposal for the biosynthesis of yohimbine alkaloids.[110]

Jiang *et al.*[98] elucidated the longstanding biosynthetic route to reserpine (**11**) (Scheme 5). Working in *Rauvolfia verticillata*, they demonstrated that the pathway proceeds *via* strictosidine (**80**) with a C-3α configuration rather than through vincoside, overturning earlier assumptions. The critical C-3β stereochemistry is generated through a two-step enzymatic epimerization mediated by a flavin-dependent oxidase and an NADPH-dependent reductase. The sequential construction of adjacent chiral centers resulted from coordinated action across distinct enzyme families. First, the flavin-dependent oxidase

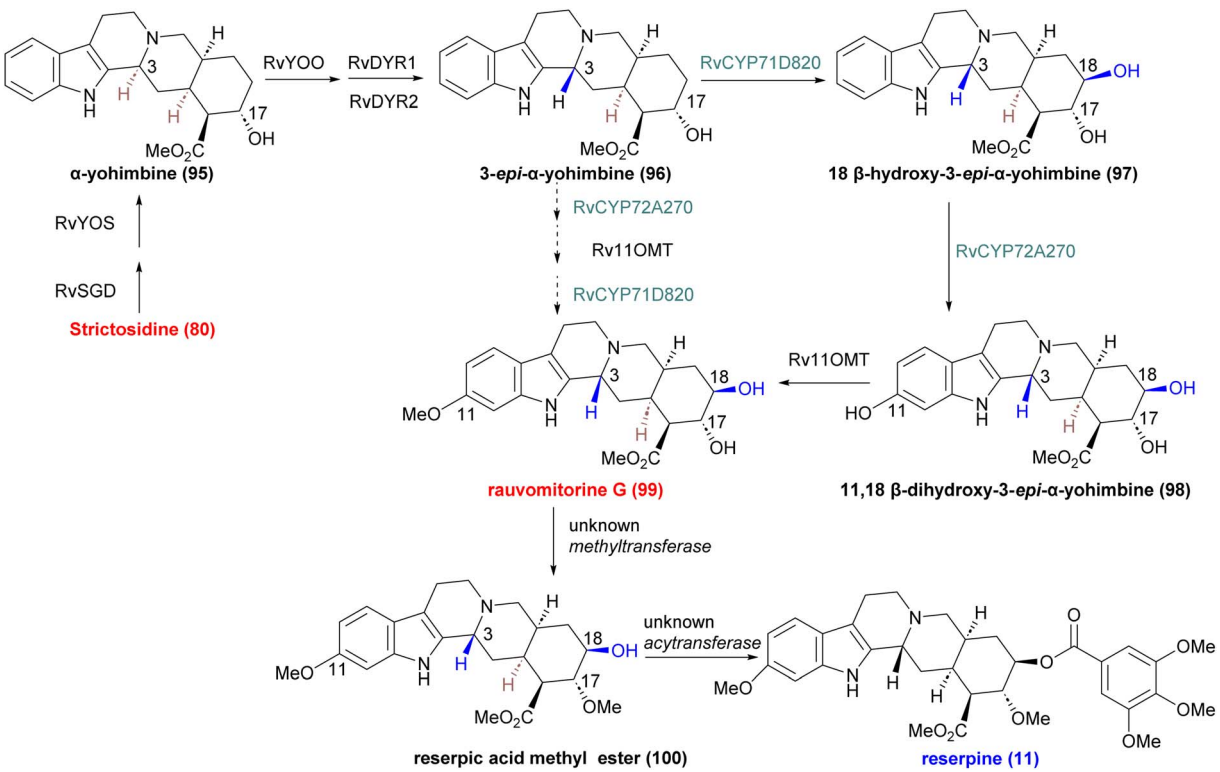

Scheme 5 The biosynthesis of reserpine by Jiang's group.[98]

RvYOO oxidizes α-yohimbine (**95**) to an iminium intermediate; this is stereoselectively reduced by the NADPH-dependent reductase RvDYR to yield 3-*epi*-α-yohimbine (**96**). Additional stereocenters and functional groups are introduced by downstream enzymes: RvCYP71D820 catalyzes 18β hydroxylation to form the fifth consecutive chiral center, while RvCYP72A270 and Rv11OMT mediate C-11 hydroxylation and *O*-methylation, producing to rauvolmitotine G (**99**), a late-stage intermediate containing all requisite stereochemical elements of reserpine (**11**). This work represents the first complete delineation of the enzymatic logic underlying reserpine's stereochemical assembly. It reveals that nature employs a modular, cooperatively acting set of enzymes for stereocontrol—distinct from synthetic strategies that typically rely on conformational biasing or late-stage epimerization. Furthermore, the identification of a conserved oxidase–reductase pair for C-3 epimerization across multiple MIA-producing plants suggests a generalized mechanism for stereochemical inversion in indole alkaloids biosynthesis. Despite substantial pathway reconstruction, several steps remain unresolved. The enzymes responsible for 17-*O*-methylation and the final 3,4,5-trimethoxybenzoylation remain unidentified, likely due to the specialized substrate requirements of the corresponding acyltransferases and the difficulty of expressing active serine carboxypeptidase-like enzymes in heterologous hosts. Additionally, the low catalytic efficiency of RvYOS and the complexity of the multienzyme pathway impeded complete reconstitution in *Nicotiana*, highlighting the need for optimized expression systems or targeted enzyme engineering.

O'Connor *et al.*[111] recently characterized the core biosynthetic steps responsible for scaffold construction in mitragynine (**1**) and related corynanthe-type alkaloids (Scheme 6). Their work also elucidated the mechanistic basis for formation of the key C-20 stereocenter. Through structural modeling and targeted mutagenesis, they identified seven amino acid residues (T53F, I100M, S116N, SGAS295-298 → ATGG) that govern stereoselectivity at this position. Unlike the dihydrocorynantheine synthase from *Cinchona pubescens* (CpDCS),[112] which exclusively generates the (20*R*) isomer, MsDCS1 (dihydrocorynantheine synthase from *M. speciosa*) produces both (20*S*) (**105**) and (20*R*) (**101**) forms, with a pronounced bias toward (20*S*). These insights were applied to achieve enzymatic production of mitragynine (**1**), its C-20 epimer speciogynine (**104**), and fluorinated derivatives. However, the enzyme responsible for C-9 methoxylation remains unidentified, representing a key unresolved step in mitragynine (**1**) biosynthesis.

Qu *et al.*[113] concurrently elucidated the biosynthetic route of kratom alkaloids in *M. speciosa*, focusing on stereoselective control through mutagenesis of MsDCS1, thereby providing a more comprehensive understanding of pathway (Scheme 7). They identified and functionally characterized nine reductases (MsDCS1–4, CoDCS, MpDCS, and others) responsible for converting strictosidine aglycone into either (20*R*)-demethylcorynantheidine (**110**), the precursor to mitragynine (**1**), or (20*S*)-demethyldihydrocorynantheine (**107**), the precursor to speciogynine (**104**). Notably, the study uncovered a previously

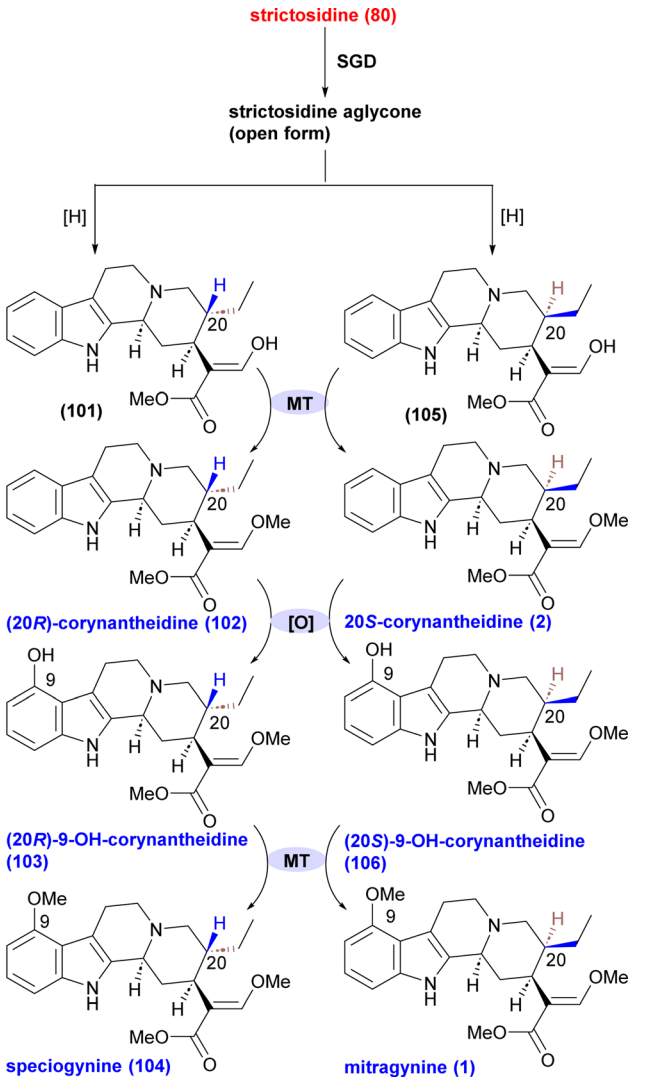

Scheme 6 The proposed pathway toward major kratom alkaloids.[111]

unknown SABATH-family methyltransferase, MsC17OMT, which catalyzes an unprecedented methylation of a non-aromatic enol at C-17—an enzymatic activity not previously observed in plant natural product biosynthesis. Using 4-hydroxytryptamine as an unnatural substrate, the authors demonstrated the enzymatic formation of demethylmitragynine (**111**) and demethylspeciogynine (**109**) through a coupled reaction cascade involving CrSTR, CrSGD, the reductases, and MsC17OMT. Finally, the leaf proteins from *Hamelia patens* were shown to methylate these intermediates into mitragynine (**1**) and speciogynine (**104**), confirming that the terminal *O*-methylation step is *S*-adenosylmethionine-dependent.

These insights reinforce the promise of engineered microbial systems for sustainable MIAs production, while also emphasizing the need for deeper optimization of enzyme expression, substrate channeling, and pathway-level regulatory control to achieve commercially competitive yields. Despite substantial progress, major bottlenecks persist. Functional characterization of numerous pathway enzymes—particularly, CYPs, and diverse transferases—remains incomplete,

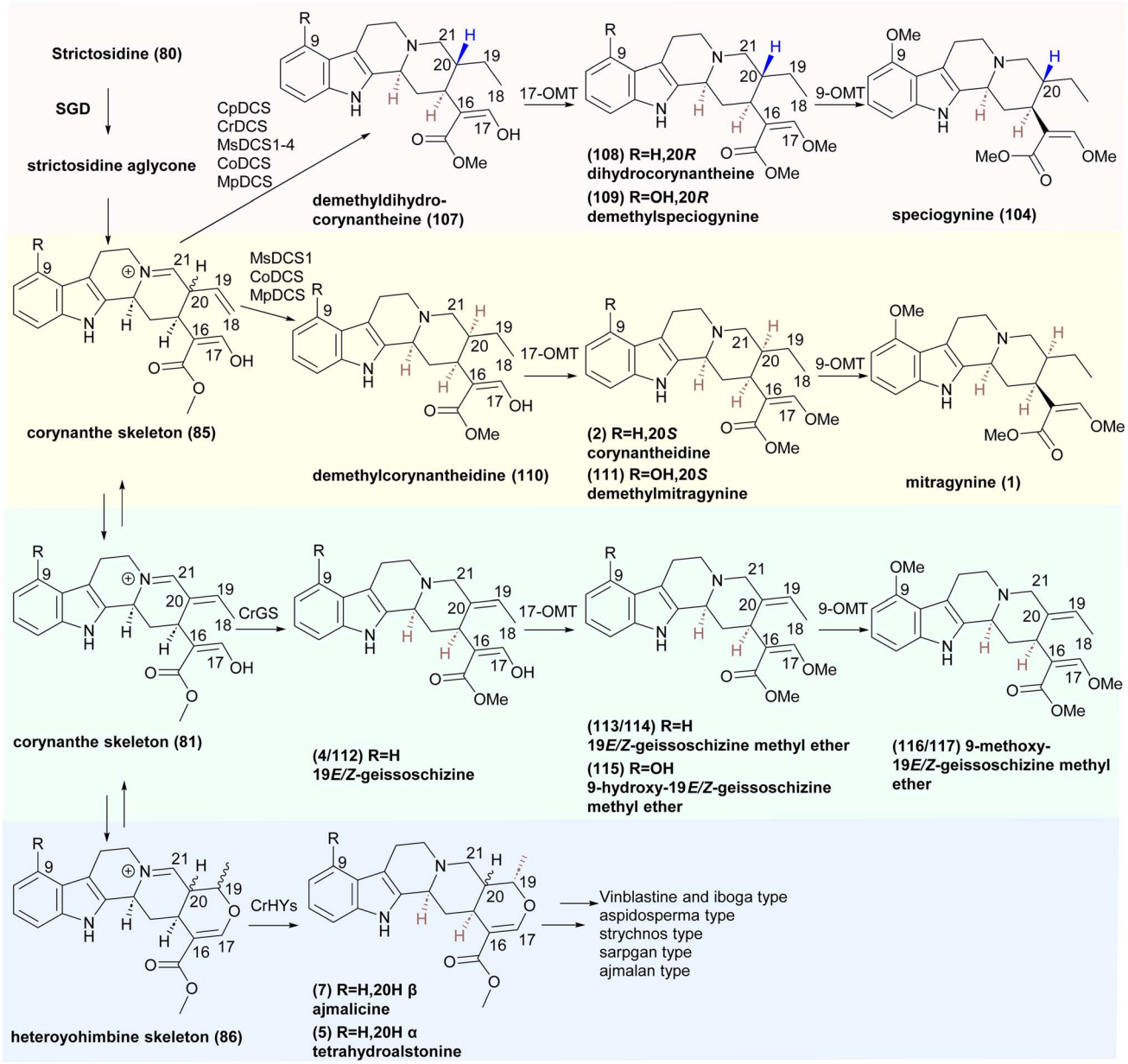

Scheme 7 The biosynthesis of kratom alkaloids by Qu's group.[113]

restricting the reconstruction of full biosynthetic routes in heterologous hosts. Cellular compartmentalization adds further complexity.[114] STR and SGD localize to the vacuole, whereas geraniol 10-hydroxylase resides on the endoplasmic reticulum (ER). Re-establishing this spatial organization in microbial or plant cell factories is technically challenging and frequently results in pathway leakage or undesired side-product formation. Additionally, intrinsic enzyme promiscuity and substrate competition can depress product titers and complicate metabolic engineering strategies. Overcoming these challenges will require integrative approaches that merge multi-omics, structural biology, and synthetic biology to clarify enzyme mechanisms, enhance catalytic performance, and build robust microbial platforms capable of scalable MIA production.

4 Synthesis

Natural products continue to serve as a cornerstone for therapeutic discovery, as exemplified by the development of numerous clinically successful drugs.[115] Among these, corynanthe alkaloids are particularly notable for their extensive stereochemical diversity—a feature that significantly enhances their utility in modern drug screening campaigns.[116] Yet systematic exploration of stereoisomeric scaffolds within compound libraries remains limited.[117,118] A prominent example is yohimbine, whose stereoisomeric derivatives show potent activity against cancer-associated G-protein-coupled receptors (GPCRs), displaying antagonistic profiles distinct from the parent molecule.[119] This underscores the value of

stereochemical tailoring in enhancing the therapeutic potential of natural products. In parallel, targeted derivatization strategies, such as halogenation, have effectively reduced adverse effects, including toxicity, while enhancing bioactivity.[120] For instance, fluorinated derivatives of vincristine—a monoterpenoid indole alkaloid—exhibit promising improvements in pharmacological performance. Collectively, these advances highlight the transformative potential of stereochemical diversification and rational derivatization in unlocking new opportunities for natural-product-based drug discovery.[121,122]

4.1 The synthesis of simple corynanthe alkaloids

The stereoselective construction of chiral centers—particularly the interplay between the C-3 stereocenter and the adjacent C15/C16/C20 stereogenic array embedded within the tricyclic ring system—remains a central challenge in the synthesis of complex MIAs. Traditional synthetic routes typically rely on late-stage functional-group manipulations of preassembled piperidine or decahydroquinoline frameworks to install the required stereochemistry. However, these methods face inherent limitations: conformational flexibility within the six-membered ring often compromises stereocontrol, generating mixtures of C3 and/or C15/C16 diastereomers that demand labor-intensive chromatographic separation.[123] Earlier approaches predominantly employed biomimetic strategies, chiral-pool starting materials, or classical thermal and radical cyclizations. Prior to modern asymmetric catalysis, syntheses frequently began from chiral natural products to enforce stereocontrol—D-tryptophan being the most common due to its ready provision of the chiral indole-ethylamine motify. Occasionally, terpenes or carbohydrates, served as alternative chiral precursors for introducing stereocenters into the non-tryptamine substructure.

4.1.1 Cook's synthesis of mitragynine. Following the successful synthesis of (−)-corynantheidine (**2**), (−)-corynantheidol (**166**), and (+)-geissoschizine (**4**) in 2000,[124] Cook and co-workers[125] advanced the first catalytic, enantiospecific total syntheses of the opioid agonist mitragynine (**1**) in 2007 (Scheme 8). A key breakthrough was their optimized Larock heteroannulation between Boc-protected 2-iodo-3-methoxyaniline (**118**) and TMS-alkyne (**119**), which delivered the 4-methoxy N^a–H indole (**120**) in 82% yield and enabled an efficient 50 g-scale preparation of 4-methoxy-D-tryptophan ethyl ester (**121**) in 91% yield following hydrolysis. This transformation effectively resolved a longstanding bottleneck in indole alkaloid synthesis. From **121**, stereocontrol was secured *via* an asymmetric P–S cyclization to set the C3 stereochemistry,

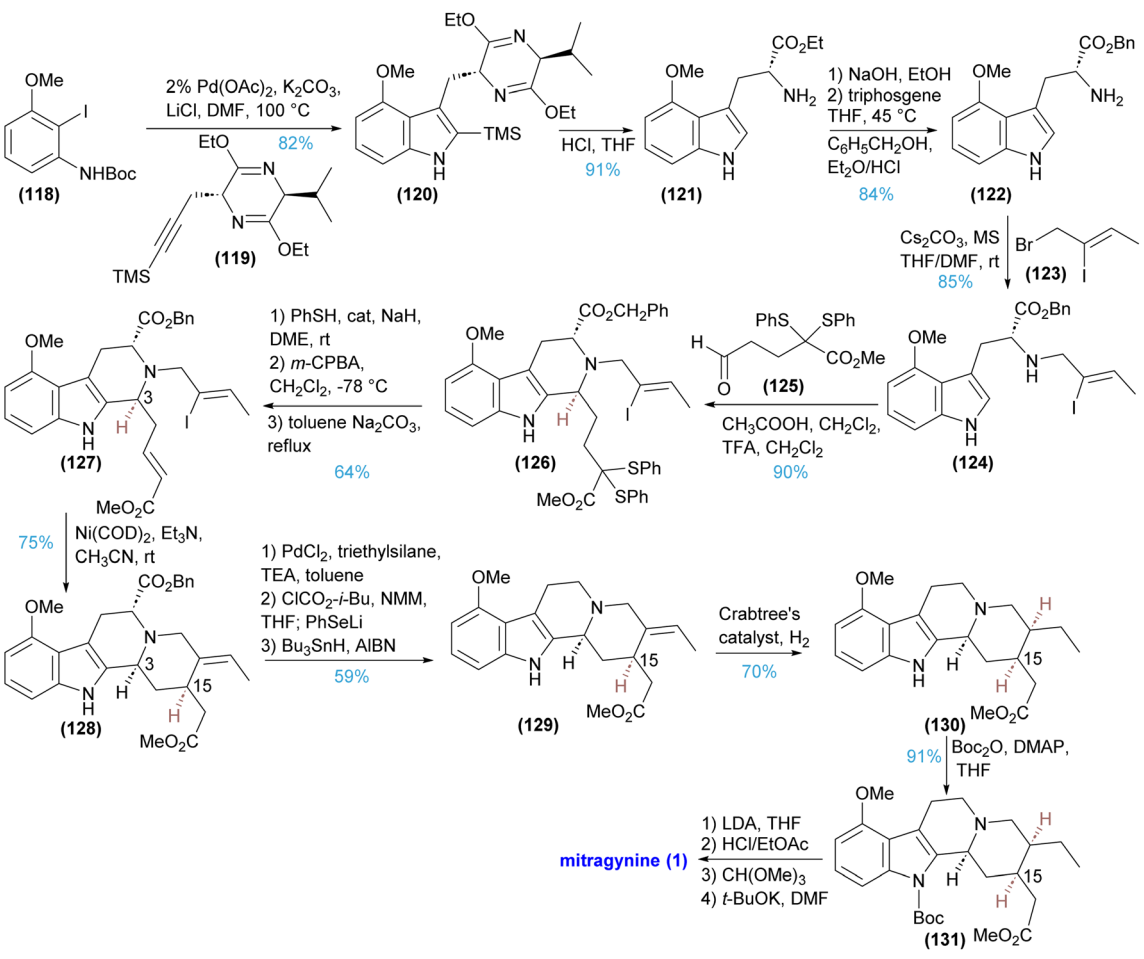

Scheme 8 Total synthesis of the opioid agonistic indole alkaloid mitragynine.[125]

followed by a $Ni(COD)_2$-mediated cyclization of **127** to furnish the corynanthe framework (**128**) with the requisite *cis* C3–C15 fusion in 75% yield. A convergent strategy from tetracyclic ester (**129**), accessed from **128** through Barton–Crich decarboxylation, enabled efficient elaboration to all target structures: reduction afforded **130**, **131**, and mitragynine (**1**) was completed through formylation and acetal-forming sequences. Notably, the methoxy substituent proved found essential for analgesic activity. Mitragynine (**1**) acts as a full agonist at μ- and δ-opioid receptors, whereas its desmethyl analog—despite high μ-receptor affinity—only a partial agonist. In contrast, the desmethoxy analog of mitragynine (**1**), corynantheidine (**2**), lacks opioid agonist activity, but reverses morphine-suppressed twitch contraction, consistent with its role as an opioid receptor antagonist. Collectively, Cook's studies demonstrated that a sterically demanding Nb-substituent is crucial for achieving complete diastereocontrol in the P–S step. Nonetheless, the route relies heavily on protecting groups (*e.g.*, Boc and benzyl esters), adding synthetic overhead and introducing opportunities for side reactions and yield erosion.

4.1.2 Martin's synthesis of dihydrocorynantheol. In 2006, Martin *et al.*[126] developed an alternative early-stage strategy that efficiently constructed the key intermediate **142** through a one-pot ring-closing metathesis–carbomagnesiation sequence (Scheme 9). They further demonstrated that TMSCl is a critical additive for enhancing the diastereoselectivity of 1,4-additions to unsaturated lactams with organocuprates, enabling concise total syntheses. Subsequent conversion of **144** to **145** *via* Bischler–Napieralski (B–N) cyclization/reduction and 9-BBN-mediated hydroxylation furnished dihydrocorynantheol (**146**) in 19% overall yield. However, despite its elegance, this approach does not readily extend to collective synthesis of diverse corynanthe alkaloids, structural optimization of the core keleton is required to accommodate the breadth of substitution patterns across the family.

4.1.3 Sato's synthesis of (−)-corynantheidine. In 2011, Sato *et al.*[127] reported the total synthesis of the indole alkaloid (−)-corynantheidine (**2**), featuring a nickel-catalyzed carboxylative cyclization with CO_2 incorporation as the central transformation (Scheme 10). The route begins with a *cis*-selective P–S reaction between L-tryptophan methyl ester (**147**) and aldehyde (**148**), establishing the requisite tetrahydro-β-carboline core with the correct configuration. The resulting advanced intermediate, enyne (**156**), was then subjected to the key Ni^0-mediated carboxylative cyclization. A major achievement of this work was the development of both stoichiometric and catalytic variants of the transformation: using $Ni(cod)_2$ and DBU under a CO_2 atmosphere, the reaction effected regio- and diastereoselective CO_2 incorporation to generate the carboxylic acid precursor to ester (**157**) with excellent diastereoselectivity. Importantly, the authors also realized a catalytic system (20 mol% $Ni(cod)_2$), furnishing the product in 58% yield and demonstrating a rare proof-of-concept for catalytic CO_2 utilization in complex-molecule synthesis. Nonetheless, the catalytic protocol was limited by its reliance on large excesses of DBU and Et_2Zn, which reduced atom economy and operational practicality.

4.1.4 Ma's synthesis of corynantheidol, dihydrocorynantheol, and mitragynine. Ma *et al.*[128] later introduced an organocatalytic platform centered on an *O*-TMS-diphenylprolinol-catalyzed Michael addition of *n*-butanal to alkylidene malonate **160**, delivering chiral aldehyde **162** (Scheme 11). This aldehyde serves as a versatile linchpin for divergent

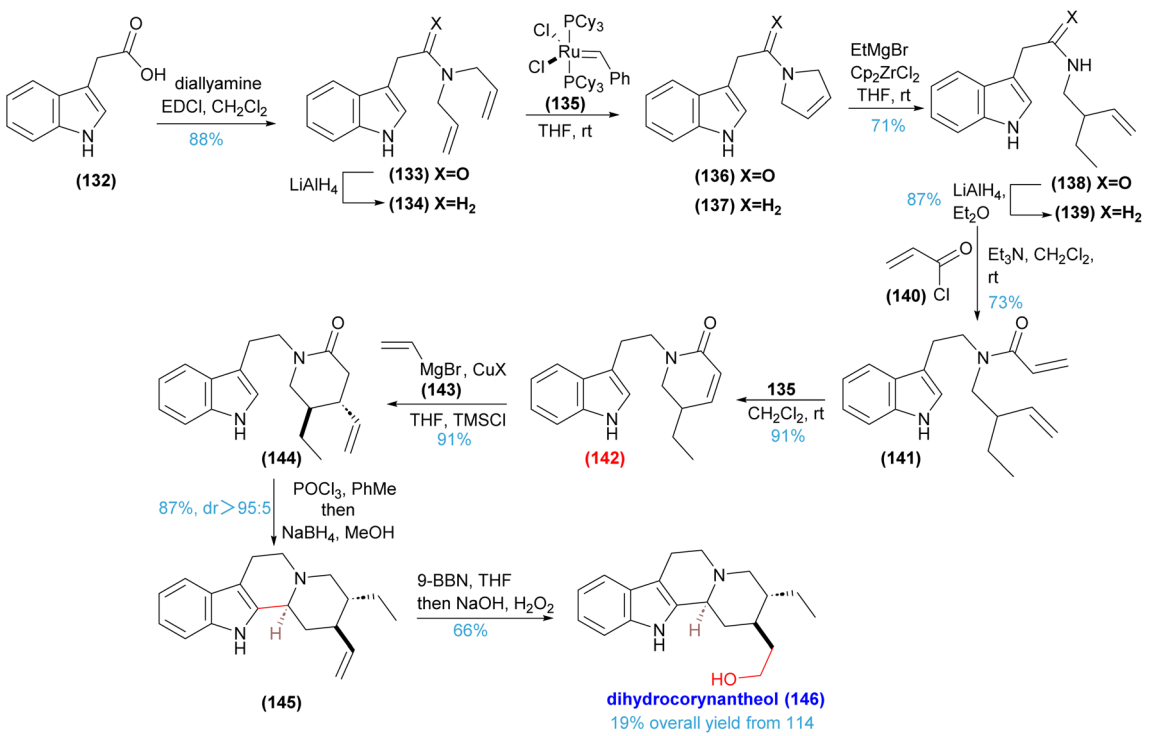

Scheme 9 Martin's general strategy for the syntheses of corynanthe alkaloids.[126]

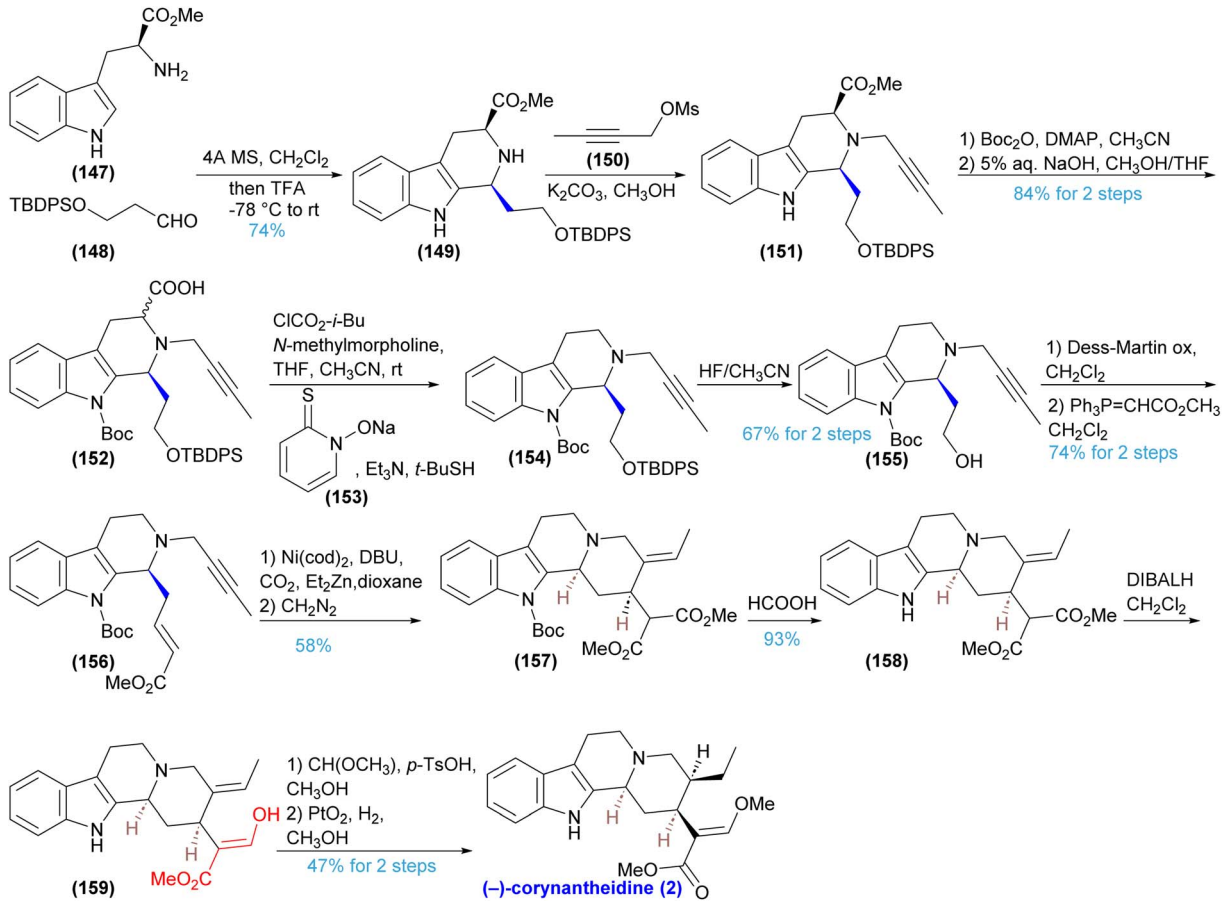

Scheme 10 Sato's total synthesis of (−)-corynantheidine by nickel-catalyzed carboxylative cyclization of enynes.[127]

syntheses of secologanin-derived tryptamine and dopamine alkaloids. Reductive amination of **162** with tryptamine (**79**), followed by spontaneous lactamization, enabled a multistep sequence to corynantheidol (**166**) and dihydrocorynantheol (**168**) *via* saponification/decarboxylation, B–N cyclization, reduction, and debenzylation. Alternatively, condensation of **162** with 4-methoxytryptamine (**169**) provided enamine **170**, which underwent diastereoselective hydrogenation, saponification/decarboxylation, and oxidation to furnish ester **172**, completing a formal synthesis of mitragynine (**1**) *via* **173**. However, enantioselectivity declined markedly upon 1 mmol scale-up from 91% to 81.6% *ee*, while diastereoselectivity in the reductive amination remained modest, necessitating chromatographic separation of isomeric mixtures. Epimerization during decarboxylation, further reduced overall efficiency. Future optimization could include screening second-generation iminium or hydrogen-bonding catalysts—potentially under continuous-flow conditions—to achieve >95% *ee* at gram scale; replacing $NaBH(OAc)_3$ with engineered transaminases or imine reductases to minimize epimerization during reductive amination; and implementing telescoped, one-pot deprotection/cyclization sequences in flow to reduce protecting-group manipulations and solvent usage by ≥ 70%.

4.1.5 Scheidt's synthesis of (−)-corynantheidine and (−)-corynantheidol. In 2024, an improved platform was reported for the synthesis of (−)-corynantheidol (**166**) and (−)-corynantheidine (**2**) (Scheme 12).[6] The route begins from compound **174**, which is converted to tertiary amine **179** on multigram scale through a concise three-step sequence. Regioselective reduction of the axial linear ester in **180** was achieved using Corey's protocol: treatment with preformed bis(dimethylaluminum) 1,2-ethanedithiolate provided ketene dithioacetal **181** in 72% yield, followed by Raney-nickel reduction to give **182** (79% yield). A Mikolajczyk-type homologation of **182**—involving *in situ* aldehyde formation using LDBBA at 0 °C—furnished homologated product **185** in 70% yield. Subsequent methanolysis of **185** with HCl at 50 °C then afforded Cook's intermediate **186** in 94% yield.[124] From intermediate **186**, (−)-corynantheidol (**166**) was obtained *via* $LiAlH_4$ reduction in 90% yield (8 steps, 18% overall). For (−)-corynantheidine (**2**), an optimized Claisen reaction (0 °C, 20 min) followed by methylation with K_2CO_3 and Me_2SO_4 in acetone furnished **2** with high diastereoselectivity (>20 : 1 E/Z) in 67% yield across two steps (9 steps, 13% overall). Building on the group's prior foundation, this updated platform addresses greater structural and functional-group complexity and provides unified access to diverse heterocyclic cores, offering enhanced potential for broad SAR exploration in medicinal chemistry.

4.1.6 Smits's synthesis of stisirikine and dihydrostisirikine. Recently, a stereodivergent Ireland–Claisen

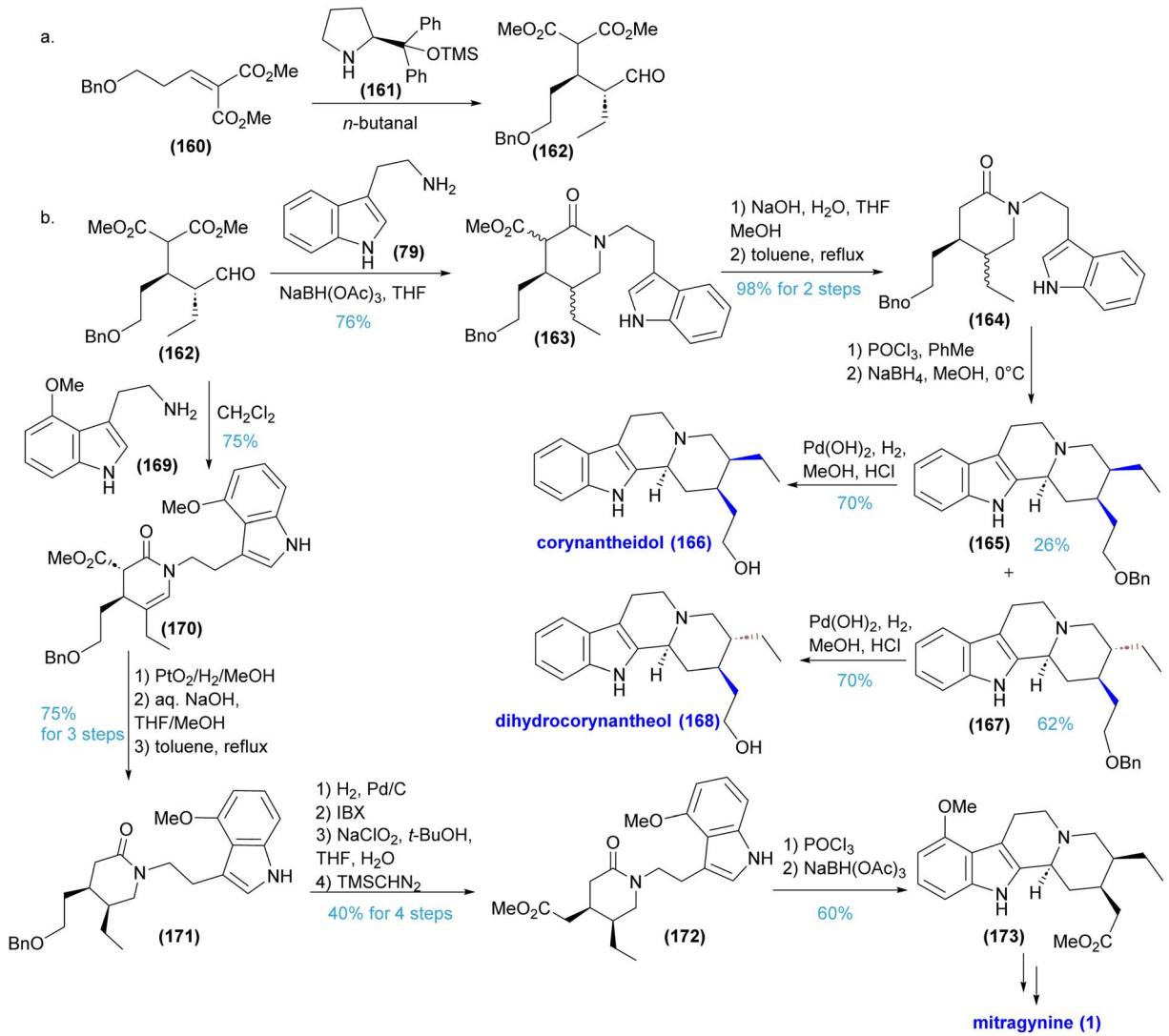

Scheme 11 An organocatalytic asymmetric synthesis of corynantheidol, dihydrocorynantheol and mitragynine using TMS-diphenylprolinol catalysis by Ma's group.[128]

rearrangement of achiral lactones catalyzed by chiral diazaborolidines enabled access to all four enantiopure stereoisomers of 3,4-disubstituted piperidines and pyrrolidines (Scheme 13).[129] In this sequence, acid **188** undergoes an Arndt–Eistert homologation to furnish **189**, which is then alkylated with bromide **191**—bearing a Boc-protected indole to oxidative degradation—to give **193**. Iodine-mediated oxidation of the amine provides the corresponding lactam in 40% yield, and subsequent B–N cyclization effects Boc, deprotection and affords **194** in 80% yield. Treatment of **194** with lithium diisopropylamide and methyl formate, followed by reduction, produces sitsirikine (**195**), and Pd-catalyzed hydrogenation of **195.** delivers dihydrositsirikine (**196**). While the route is commendable for its stereodivergence and modularity, several drawbacks persist, including variable efficiency in the key rearrangement step and reliance on stoichiometric quantities of chiral auxiliaries rather than catalytic asymmetric induction.

4.1.7 Zhang's collective synthesis of corynanthe alkaloids. In 2024, Zhang *et al.*[130] reported a collective synthesis of diverse corynanthe alkaloids from a shared intermediate incorporating a chirality-tunable structural unit. Central to the strategy is stereodivergent diastereoselective hydrogenation at C15 and C20, directed either by a primary alcohol or by a *p*-methoxybenzyl (PMB) protecting group functioning as a steric shielding moiety (Scheme 14). The synthesis of **207** begins with oxidation of known precursor **197** using $POCl_3$ in DMF to provide aldehyde **198** in 70% yield. Condensation of **198** with (*S*)-*tert*-butanesulfinamide, generates an *N*-sulfinyl imine, which undergoes a vinylogous Mannich addition with the lithium dienolate of dioxinone **201** formed *in situ* with LiHMDS to afford predominantly diastereomer **202.** After sulfinyl deprotection and C-ring closure, a Mannich cyclization (formaldehyde/$KHSO_4$) furnishes pentacyclic intermediate **203** in 76% yield over two steps. Treatment of **203** with NaOMe gives ester **204** (85% yield), which is then TBS-protected, reduced with DIBAL-H, and

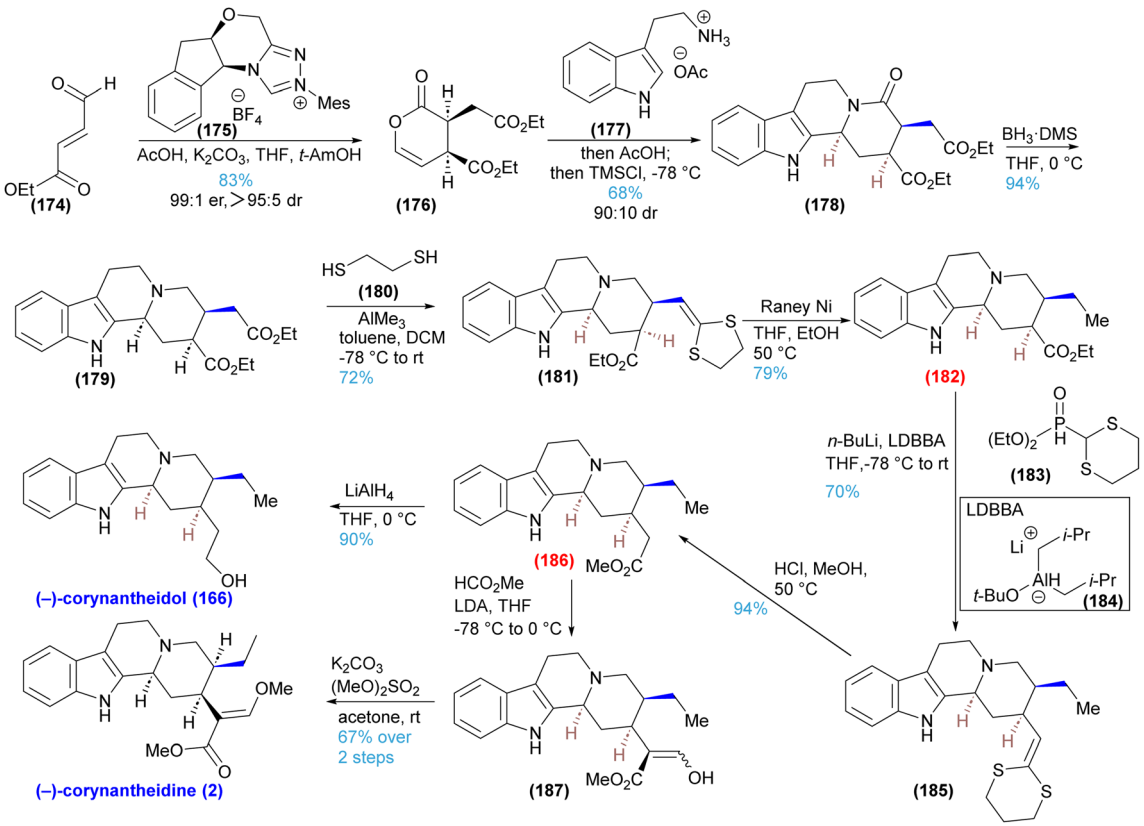

Scheme 12 A generalizable synthetic platform for the synthesis of corynantheine alkaloids by Scheidt's group.[6]

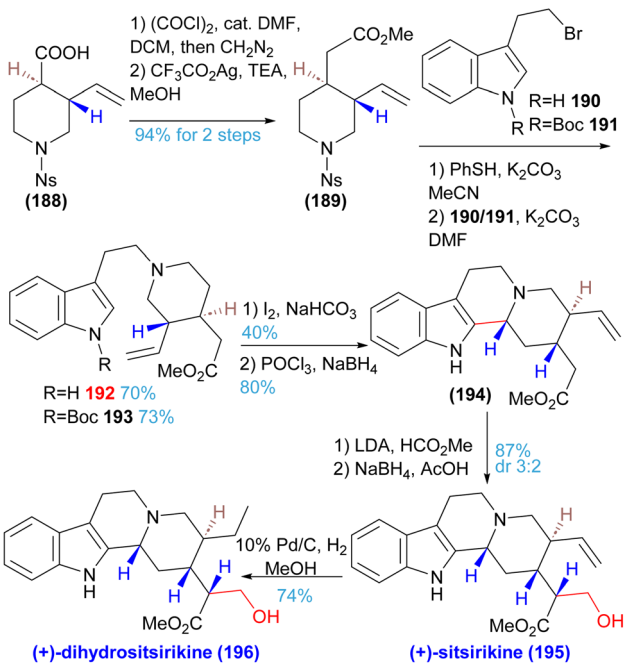

Scheme 13 Smits's enantiopure piperidines *via* stereoselective Ireland–Claisen rearrangement to achieve corynanthe alkaloid.[129]

deprotected with TBAF to produce ketone **205** in 73% yield over two steps; its structure was confirmed by X-ray crystallography. A–Horner–Wadsworth–Emmons olefination of ketone **205** subsequently delivers the key common intermediate **206** in 96% yield. Leveraging the tunable stereochemical features of **206**—including the PMB shielding effect and the directing role of the primary alcohol—the authors synthesized four distinct classes of corynanthe alkaloid subclasses *via* tailored downstream sequences. Despite its versatility, the approach exhibits several limitations. Extensive oxidant screening was required for the conversion of **207**, with the Parikh–Doering oxidation emerging as the sole viable option but causing undesired double-bond migration. In addition, poor chemoselectivity toward aldehyde addition in the presence of ester groups rendered classical nucleophiles such as MeLi and MeMgBr unsuitable, necessitating the use of Me_3Al and thereby narrowing reagent scope. Several steps also proceeded with only moderate efficiency; for example, the synthesis of hirsuteine (**212**) achieved only 43% yield over two steps. To address these issues, potential improvements in optimization strategies are proposed, such as: developing tailored oxidants to prevent double-bond migration during the oxidation of **207**, designing advanced directing groups (*e.g.*, siloxy-based motifs) to enhance the selectivity of Me_3Al-mediated additions, and systematically optimizing reaction conditions in low-yielding transformations.

4.1.8 Al-Khrasani, Szilard, and Soós's synthesis of mitragynine pseudoindoxyl and speciogynine pseudoindoxyl. Al-Khrasani, Szilard, and Soós *et al.*[131] reported the first enantioselective total synthesis of the potent μ-opioid receptor agonists mitragynine pseudoindoxyl (**236**) (Scheme 15). Their

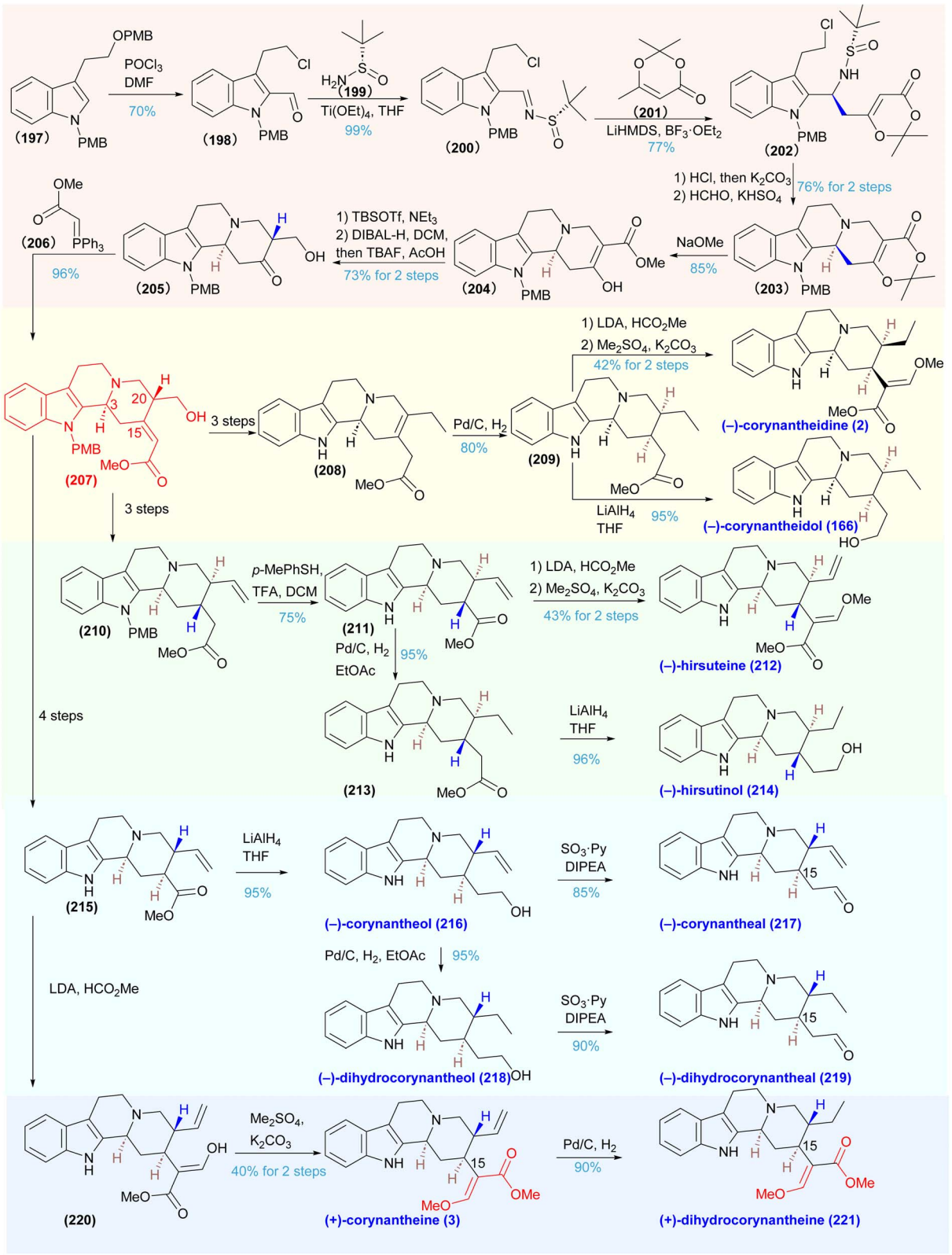

Scheme 14 Zhang's collective synthesis of corynantheine alkaloids.[130]

bioinspired, and protecting-group-free design converges on two key building blocks: an oxidized tryptamine-derived spiro-cyclopropyl pseudoindoxyl (**228**) and a chiral secologanin analog (**227**), the latter prepared from (−)-carvone (**222**) in seven scalable steps. The core spiro-5-5-6 tricyclic ramework is assembled through a diastereoselective cascade relay involving a transient cyclic imine (formed from **231**) that undergoes a formal [3 + 2] cycloaddition with **232** under mild conditions,

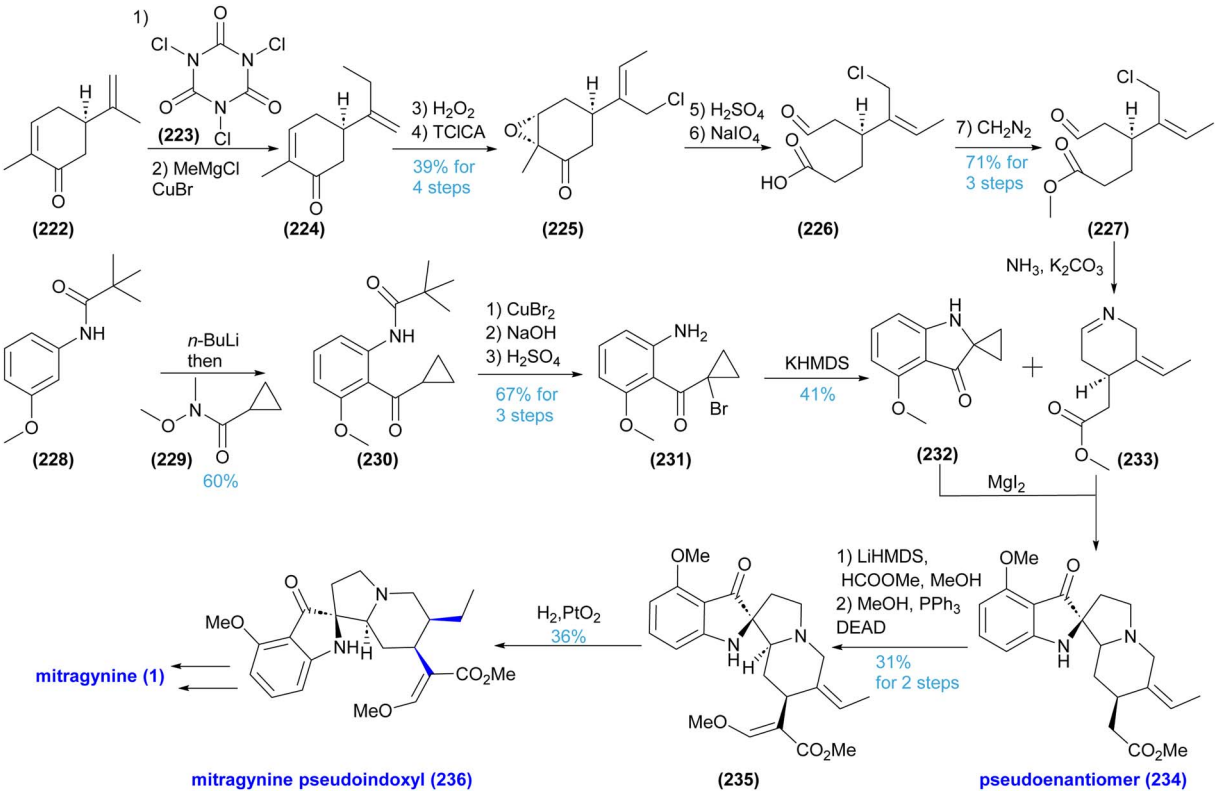

Scheme 15 The first enantioselective and scalable total synthesis of mitragynine pseudoindoxyl by Al-Khrasani, Szilard, and Soós's group.[131]

simultaneously forming four bonds, two rings, and two stereocenters in a single operation. Although specialized systems such as the Adam catalyst and a hydrogen-atom-transfer reduction were employed, the final reduction step exhibited only moderate diastereoselectivity. The authors further propose that **236** exists in a dynamic equilibrium among interconverting stereoisomers in biologicalmedia, implying that its pharmacological properties may arise from a stereodynamic ensemble. However, this mechanistic hypothesis requires additional experimental verification.

4.2 Total synthesis of yohimbine alkaloids

4.2.1 Jacobsen's and Hiemstra's synthesis of yohimbine. Jacobsen *et al.* (2008)[132] reported the synthesis of yohimbine (**8**) through a 11-steps process, with 14% overall yield (Scheme 16). Their route leveraged a chiral ion-pair system formed with an anion-binding thiourea catalyst, enabling a strategic departure from the conventional E-ring-first approach. By constructing the C-ring at an early stage—followed by sequential assembly of the D- and E-rings. The authors directly addressed the long-standing challenge of installing the C-3 stereocenter when the

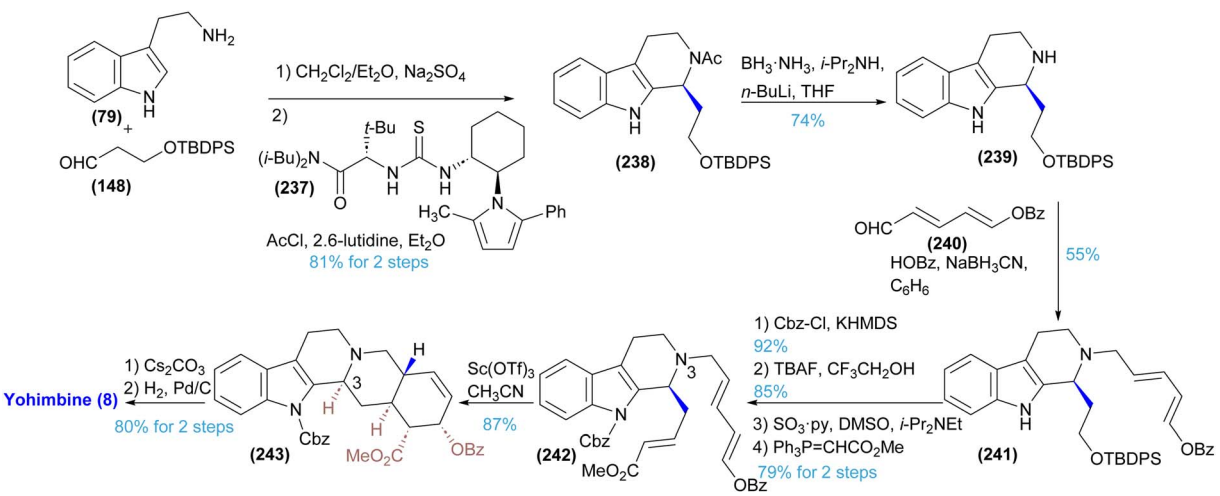

Scheme 16 Catalytic asymmetric total synthesis of (+)-yohimbine.[132]

E-ring is introduced first. Condensation of tryptamine (**79**) with aldehyde **148** furnished imine **238**, and reductive amination of **239** with aldehyde **240** afforded amine **241** in 55% yield. Subsequent *N*-protection of the indole (Cbz-Cl/KHMDS), TBDPS deprotection (TBAF), oxidation (SO_3·pyridine), and a Wittig olefination provided IMDA recursor **242** with79% yield over two steps. The $Sc(OTf)_3$-promoted IMDA of **242** then yielded cycloadduct **243**, as a single diastereomer with 87% yield. Final deprotection with Cs_2CO_3 and hydrogenation of the olefin completed the synthesis of (+)-yohimbine (**8**). Hiemstra *et al.*[133] developed a closely related strategy, likewise positioning the P–S reaction as the stereochemical control point. In contrast to Jacobsen's anion-binding thiourea system, however, they employed chiral phosphoric acid catalysis. The overall strategy paralleled Jacobsen's—early C-ring formation followed by diastereoselective Diels–Alder construction of the D- and E-rings—highlighting the growing consensus around this C-ring-first (Scheme 17).

4.2.2 Martin's synthesis of yohimbine alkaloids. Martin *et al.*[134] presented a diversity-oriented synthesis platform that combined a multicomponent assembly process (MCAP) with a dipolar cycloaddition to rapidly generate analogs of yohimbine and corynanthe alkaloid derivatives (Scheme 18). Treatment of dihydro-β-carbolines (**255**) with crotonyl chloride and *tert*-butyldimethyl(vinyloxy)silane in CH_2Cl_2 afforded amides (**258**) in 85% yield. Reaction with *N*-methylhydroxylamine hydrochloride produced a nitrone intermediate, that underwent spontaneous [3 + 2] dipolar cycloaddition, delivering single diastereoisomers (**259**). To broaden structural diversity, bromo-substituted β-carbolines (**262**, **268**) were incorporated as advanced intermediates, enabling Suzuki cross-coupling before cycloaddition and reduction, thus allowing introduction of aryl substituents and further *N*-functionalization to ureas or amides. However, the study provides no mechanistic or experimental insight into stereocontrol during the key cycloaddition or subsequent reduction steps, revealing limited command over chiral-center the construction of chiral centers. Despite claims of library-generation capability, the actual derivative scope remains comparatively narrow.

4.2.3 Sarkar's synthesis of alloyohimbane. The first selective synthesis of a yohimbane framework was reported by Palmisano in 1987[135] employing the classical sequence of D–E ring construction followed by a B–N cyclization to close the C-ring. Sarkar's approach[136] builds on this foundation, using enzymatic desymmetrization of a *meso*-diacetate to establish enantioenrichment and maintaining the traditional E-ring-first strategy (Scheme 19). The commercially available *meso*-diacetate **272** undergoes porcine pancreatic lipase (PPL)-mediated hydrolysis in pH-7 phosphate buffer containing 1 N $NaHCO_3$ (to suppress nonenzymatic background hydrolysis), producing the monoacetate **273** in >95% *ee*, and >80% yield on multigram scale. For the synthesis of (−)-alloyohimbane (**281**), **273** is converted to azide **274** *via* Mitsunobu azidation, followed by K_2CO_3-mediated hydrolysis and Staudinger reduction to give amino alcohol **275**. Coupling of **275** with 3-indolylacetic acid (EDC/HOBt) furnishes amide **276**, which after Boc protection, Mitsunobu cyanation, hydrolysis, and deprotection–cyclization yields lactam **277**. A Bischler–Napieralski cyclization followed by Pd/C hydrogenation provides (−)-alloyohimbane (**281**) in 91% yield. The same sequence enables the synthesis of (−)-yohimbane (**291**), demonstrating the generality of the strategy.

4.2.4 Gellman and Hong's synthesis of (−)-yohimbane. They both streamline asymmetric yohimbane synthesis, reducing traditional >10-step routes to 5–6 steps (Scheme 20).[137,138] Each relies on a B–N cyclization to assemble the pentacyclic core and emphasizes stereoselectivity through catalytic strategies (organocatalysis, cooperative catalysis). Both protocols use simple starting materials and avoid harsh conditions—*e.g.*, the 2017 route employed a milder B–N

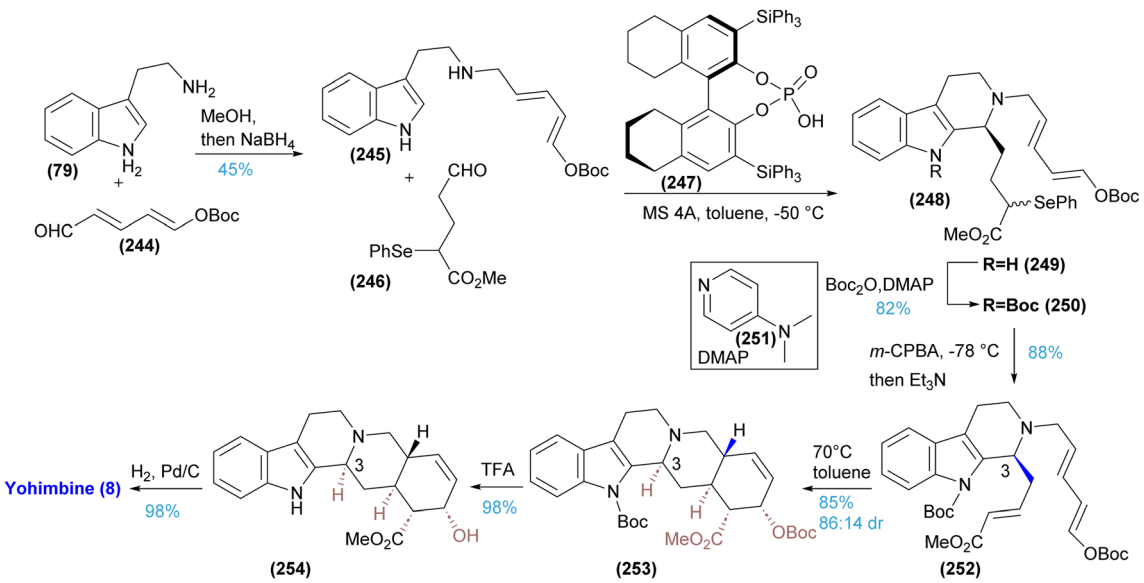

Scheme 17 Total synthesis of (+)-yohimbine *via* an enantioselective organocatalytic P–S reaction.[133]

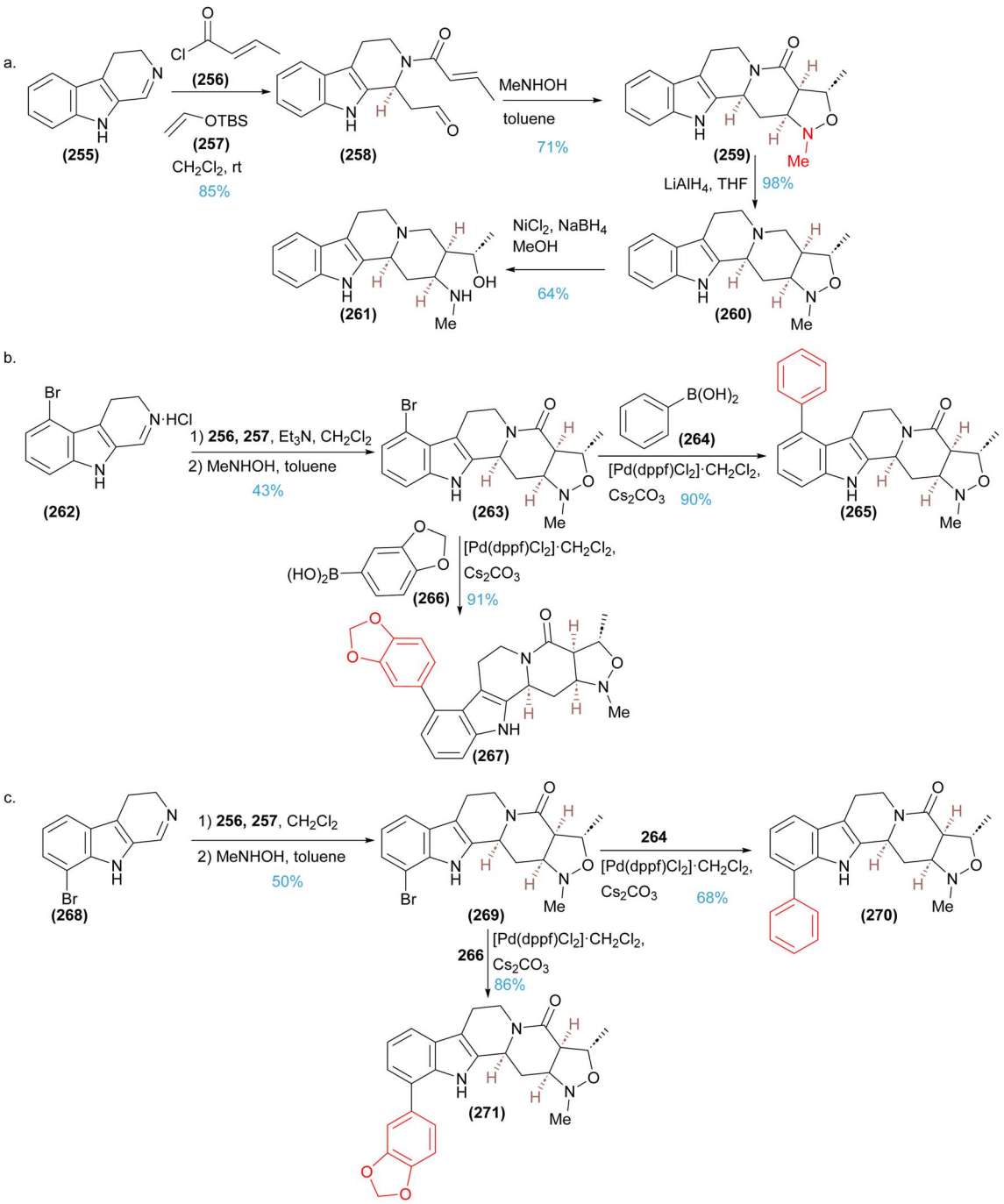

Scheme 18 A novel MCAP-cycloaddition sequence to gain rapid access to novel derivatives of yohimbine and corynanthe compounds by Martin's group.[134]

activation, while the 2020 approach used hydrogen-bond donors to suppress side reactions. In the synthesis of yohimbane (**291**),[138] the sequence begins with a copper mediated Michael addition to pyranone **286**, delivering lactone **287** in 89% yield and high diastereoselectivity (dr 12 : 1). A subsequent ring-closing metathesis with Grubbs-II catalyst, furnishes the fused *trans*-lactone **288** in 97% yield. A key advance is a modified B–N cyclization, in which the tertiary amide is activated under mild conditions using Tf_2O and 2,6-di-*tert*-butylpyridine (DTBP), circumventing classical reagents such as $POCl_3$ $LiAlH_4$ reduction then constructs the pentacyclic framework, and final hydrogenation affords yohimbane (**291**). The route proceeds in 5–6 steps from 4-pentenal (**282**) with a 50% overall yield.

In contrast to the pentenolide-based strategy of Hong *et al.*,[138] which used an organocatalytic cross-aldol/lactonization sequence to construct a versatile lactone that was subsequently elaborated *via* Michael addition and ring-closing metathesis. Gellman *et al.*[137] developed a catalytic intramolecular conjugate

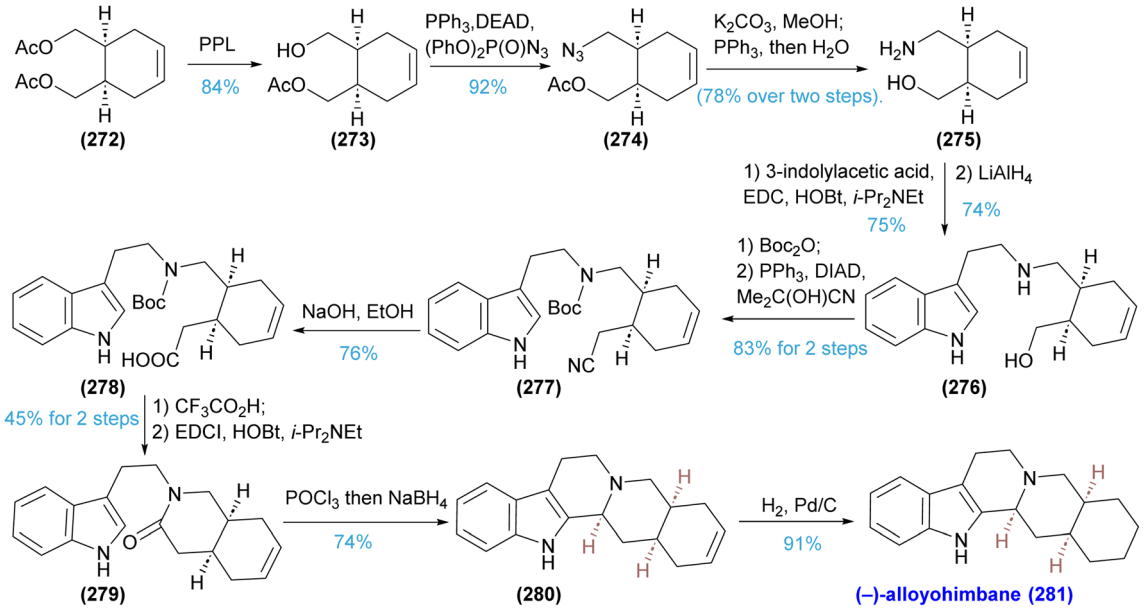

Scheme 19 Enantioselective syntheses of (−)-alloyohimbane by an efficient enzymatic desymmetrization process.[136]

addition of aldehyde-derived enamines to unactivated α, β-unsaturated esters. Their dual catalytic system employs chiral pyrrolidine (**294**) for enamine formation and a urea-based hydrogen-bond donor to activate the ester, thus addressing the intrinsic chemoselectivity challenge between conjugate addition and competing homoaldol pathways. The cyclization forms cyclohexane rings with high enantioselectivity and simultaneously sets two adjacent stereocenters. Applied to a concise six-step synthesis of (−)-yohimbane (**291**) from cycloheptene, the strategy features a one-pot reductive amination–cyclization and a B–N reaction, enabling a more direct C–C bond-forming disconnection relative to the multi-transformation sequence of Hong *et al.*

4.2.5 Scheidt's synthesis of (−)-rauwolscine and (−)-alloyohimbane. Scheidt *et al.*[139] presented a concise and enantioselective total synthesis of the yohimbine alkaloids (−)-rauwoiscine (**9**) and (−)-alloyohimbane (**281**) (Scheme 21), based on *N*-heterocyclic carbene (NHC) catalysis followed by an amidation/*N*-acyliminium ion cyclization. The route begins with an NHC-catalyzed dimerization of commercially available ethyl 4-oxobutenoate (**174**) to furnish the key enol lactone (**176**) building block in excellent enantioselectivity on multigram

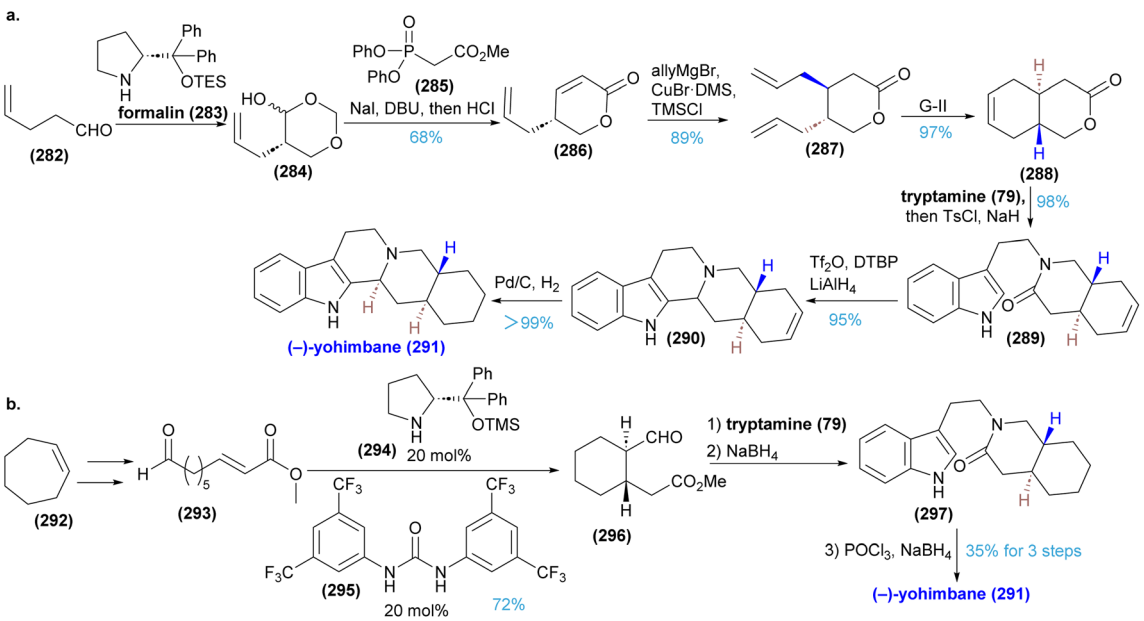

Scheme 20 The efficient asymmetric synthesis of yohimbine by Hong's group (a) [138] and Gellman's group (b).[137]

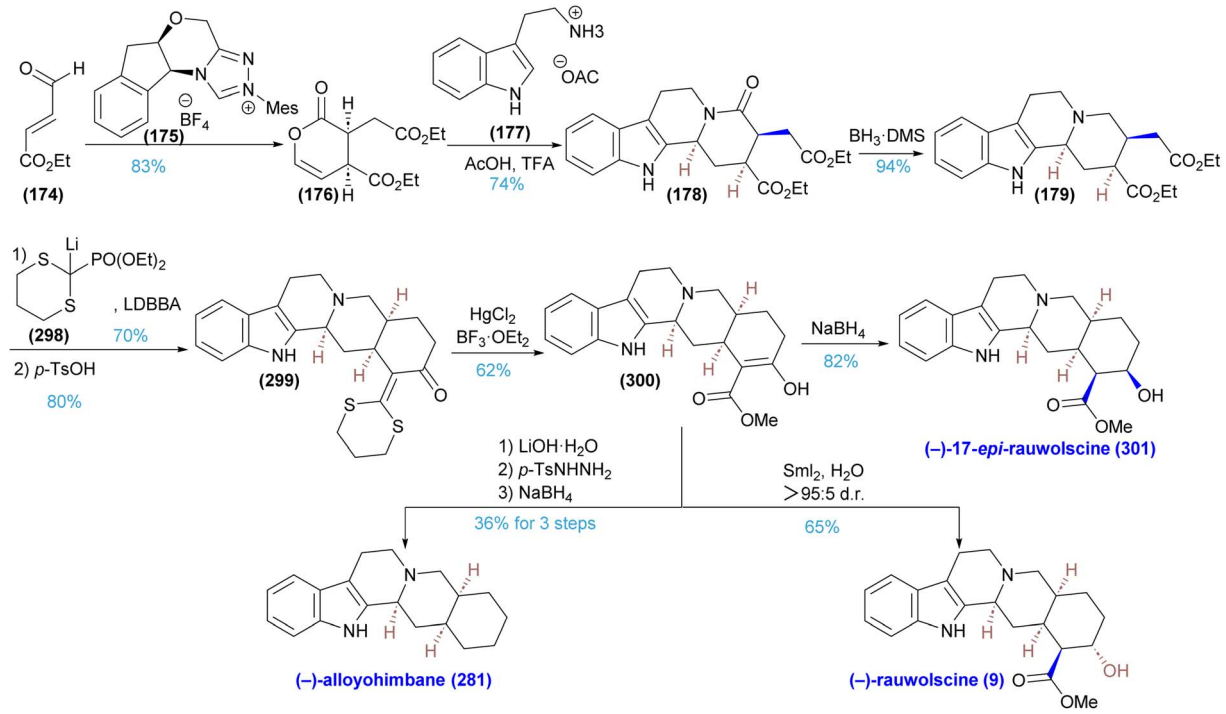

Scheme 21 A concise, enantioselective approach for the synthesis of yohimbine alkaloids by Scheidt's group.[139]

scale. This intermediate then undergoes a one-pot, protecting-group-free sequence with tryptamine, in which acylation and acid-promoted *N*-acyliminium ion cyclization to assemble the tetracyclic ABCD core of the yohimbines in a single operation, establishing three stereocenters with high diastereocontrol. After lactam reduction, a Wittig–Horner homologation extends the ester side chains, and a regioselective acid-mediated cyclization closes the E-ring; this step requires careful optimization to suppress side reactions and ensure separability of intermediates. Final diastereoselective reduction of β-ketoester (**300**) with SmI_2/H_2O provides (−)-rauwoiscine (**9**), whereas decarboxylation followed by Wolff–Kishner reduction yields (−)-alloyohimbane (**281**).

4.2.6 Zu's synthesis of stereoisomeric yohimbine alkaloids. They further reported a collective enantioselective synthesis of all four stereoisomeric subfamilies of yohimbine alkaloids using a bioinspired strategy that bypasses scarce chiral precursors such as secologanin (77) (Scheme 22).[140] The approach employs an achiral pyrone dimer (**303**), generated in a single photo-dimerization step, as a low-cost 10-carbon surrogate for secologanin. Ring-opening of the dimer affords an aldehyde that undergoes a chiral phosphoric acid-catalyzed enantioselective P–S/amidation cascade with tryptamine derivatives. This key step constructs the entire pentacyclic core while simultaneously controlling all five stereogenic centers (up to 95% *ee*). Divergent elaboration from intermediates **306** and **307** enables access to multiple natural products: venenatine (**311**) *via* hydrogenation and amide reduction; alstovenine (**309**) *via* a novel $I_2/PhSiH_3$-mediated C3-epimerization; and β-yohimbine (**314**) and pseudoyohimbine (**316**) *via* alkene isomerization, stereoselective reduction, and redox-driven C17-epimerization. Although the sequence avoids reliance on natural chiral building blocks adjustment of C20 stereochemistry (through alkene isomerization/hydrogenation) necessitates an added a C16 epimerization step. Several operations require demanding conditions, including tightly temperature-controlled C16 epimerization (15 °C) and low-tolerance steps such as Swern oxidation that employ highly sensitive reagents.

4.2.7 Enantioselective total synthesis of (+)-reserpine. Jacobsen *et al.* delivered the first effective solution to the long-standing challenge of controlling C-3 stereochemistry in the synthesis of reserpine (**11**), achieving this through a catalytic enantioselective Formal Aza–Diels–Alde reaction (Scheme 23).[141] TBS deprotection of tetracyclic intermediate **321** followed by oxidation furnished keto-aldehyde **322**, which underwent a highly efficient intramolecular enamine aldol reaction to construct the E-ring and provide pentacyclic intermediate **324**. Pinnick oxidation and diazomethane esterification yielded methyl ester **325**. The C-15 hydroxy group was transformed into α, β-unsaturated ester **326** *via* a trifluoroacetylation–elimination sequence. After extensive optimization, a cationic iridium catalyst was identified that enabled a highly diastereoselective hydrogenation (dr = 6 : 1) of the sterically congested enoate **326**, delivering saturated ester **327** with the desired *cis*-fused ring junction in 44% yield. X-ray crystallography unambiguously established the stereochemistry of **327**. Final global deprotection (PMB cleavage with TfOH and Ts removal *via* sodium–mercury amalgam), followed by esterification with 3,4,5-trimethoxybenzoyl chloride, completed the total synthesis of reserpine (**11**).

The corynanthe scaffold contains up to six contiguous stereocentrs, including the epimerization-prone C-3 and the sterically congested C-15/C-20 quaternary centrs. Although

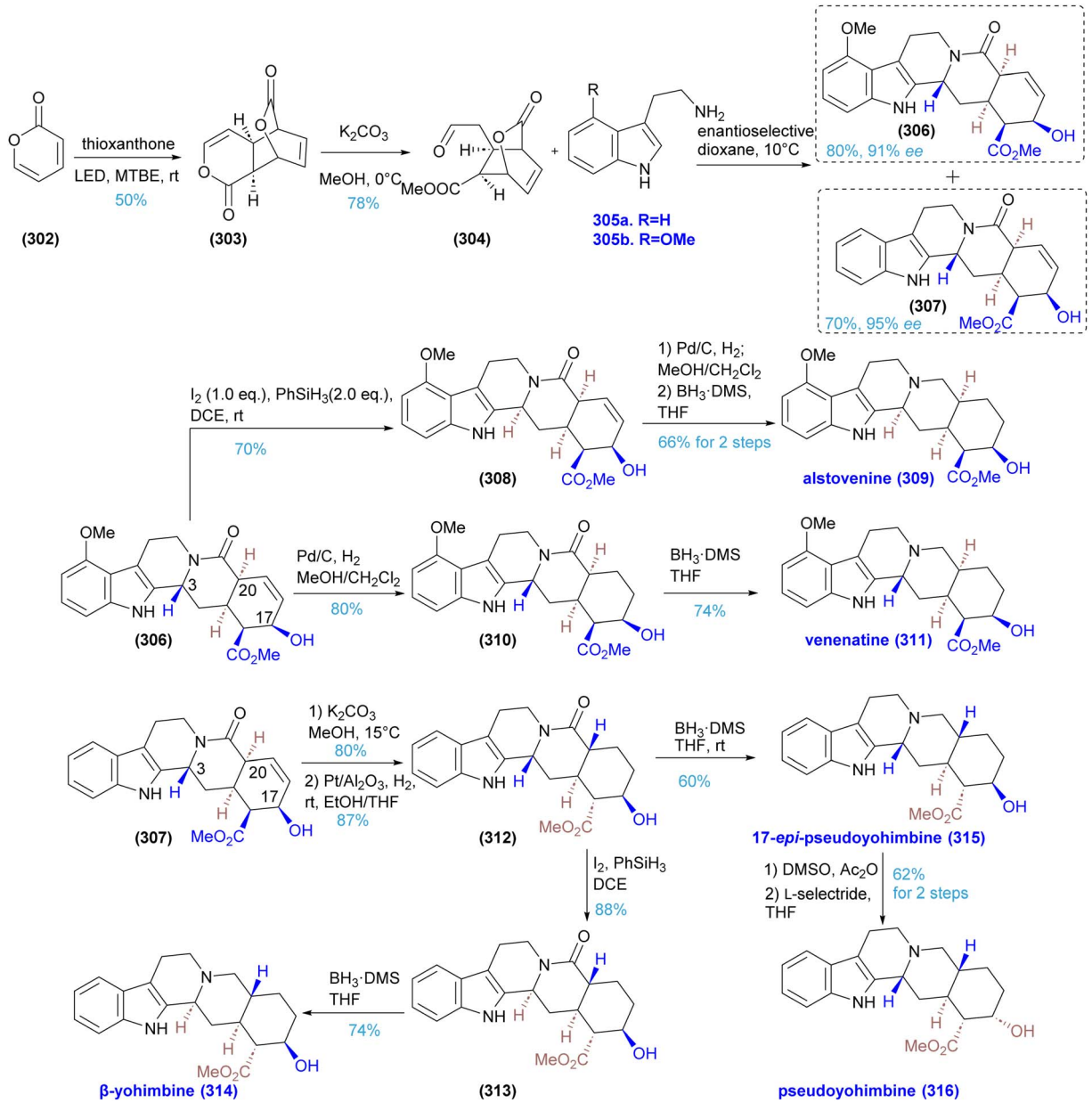

Scheme 22 Collective total synthesis of stereoisomeric yohimbine alkaloids.[140]

state-of-the-art asymmetric catalysis—organocatalytic Michael additions, iridium-catalyzed allylations or enzymatic reductions—routinely furnishes 90–95% *ee* for one or two centers, the cumulative stereopurity across full sequences often collapses to 60–80%. Construction of the indoloquinolizidine core traditionally relies on B–N or P–S cyclizations that require activated iminium or acyl-iminium intermediates formed under harsh dehydrating conditions. Such conditions compromise acid-labile substituents (vinyl, hydroxy, glycosyl) and promote indole polymerization. Metal-catalyzed C–H activation methods circumvent strong acids but provide poor regioselectivity on the congested indole framework. Recently, however, novel catalytic systems including chiral bifunctional organocatalysits and engineered enzymatic platforms have significantly improved the efficiency and selectivity of key cyclization events. Integration of asymmetric catalysis with dynamic kinetic resolution has further emerged as a powerful strategy to generate multiple stereocenters concurrently with high fidelity.

5 Activity

5.1 Anti-inflammatory

Aberrant immune responses are increasingly recognized as major drivers of inflammatory pathologies, arising from dysregulated interactions between pro-inflammatory mediators (cytokines, chemokines) and immune cell populations (macrophages, T-cells).[142,143] Yohimbine (**8**) exhibits notable *in vitro* anti-inflammatory activity, primarily through downregulation of COX-2, TNF-α, and NF-κB expression.[144] Emerging evidence also suggests chondroprotective effects against condylar cartilage

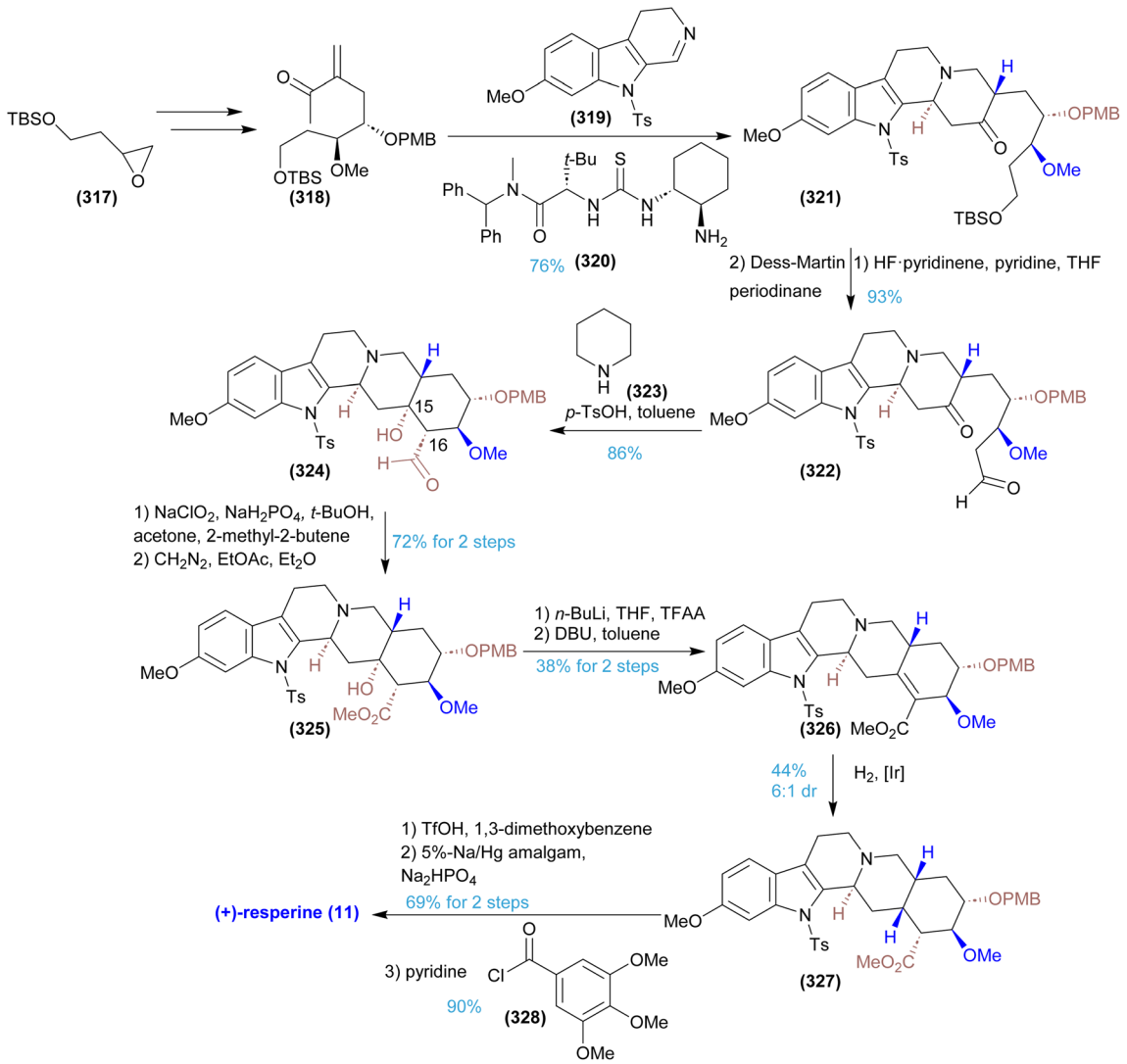

Scheme 23 Enantioselective total synthesis of (+)-resperine (**11**).[141]

degradation in both *in vitro* and *in vivo* models, potentially mediated *via* suppression of NF-κB signaling and attenuation of IL-1 or norepinephrine-induced IL-6 upregulation.[145] Mechanistic proposals implicate α_2-AR inhibition and subsequent upregulation of tyrosine hydroxylase (TH). Because α_2-AR activation lowers cyclic adenosine monophosphate (cAMP), its inhibition may restore cAMP-driven TH expression, suggesting a possible cAMP-dependent anti-inflammatory mechanism.[146–148] Rhynchophylline (**12**) suppresses microglial activation and reduces nitric oxide (NO) and prostaglandin E2 (PGE2) production,[149] while isorhynchophylline (**13**) appears to mitigate inflammation by modulating NF-κB and MAPK pathways (Table 2 biological activity of corynanthe and related alkaloids).[150] Although these findings highlight promising anti-inflammatory potential, further mechanistic clarification and translational validation are required.

5.2 Neuro-protection

The principal neuroprotective constituents identified to date are corynanthe-type and oxidized indole-type alkaloids, which exhibit a broad spectrum of bioactivities, including anti-amyloid aggregation, anti-tau hyperphosphorylation, anti-inflammatory, anti-aging, and cholinesterase-inhibitory effects.[166–169] *U. rhynchophylla*, a rich source of corynanthe alkaloids, has been widely utilized in traditional chinese medicine for treating cardiovascular and central nervous system disorders.[169,170] Ramanathan *et al.*[171] reported that the methanolic leaf extract of *Uncaria attenuata* (yellow hookah) isplayed robust cholinesterase inhibitory activity. Among the isolated compounds, villocarine A emerged as the most potent inhibitor of both acetylcholinesterase (AChE) and butyrylcholinesterase (BChE), with IC_{50} values of 14.45 μM and 13.95 μM *in vitro*, respectively. In comparison, geissoschizine methyl ether showed weaker inhibition, with IC_{50} values of 35.28 μM (AChE) and 17.65 μM for AChE and BChE *in vitro*. Molecular docking studies further revealed that villocarine A interacts with AChE *via* hydrogen bonding and h hydrophobic contacts across five key binding pockets, whereas its interaction with BChE is mediated potentially through hydrophobic interactions. Collectively, these findings position *U. attenuata* as

a promising source of bioactive alkaloids with potential applications in the management of age-related dementias. In addition, HSN (**6**) has been shown to mitigate glutamate-induced neuronal death in cultured rat cerebellar granule cells by inhibiting Ca^{2+} influx.[172] Yohimbine (**8**), anestablished α_2-adrenergic receptor antagonist, has demonstrated clinical utility as an antidote for severe amitraz poisoning, facilitating rapid neurological recovery, preventing bradycardia, and supporting hemodynamic stability.[173] Nevertheless, the clinical evidence for supporting its broader neuroprotective efficacy remains preliminary.

5.3 Cardiovascular activities

Ajmaline (**10**) has been proposed to exert antiarrhythmic effects through modulation of potassium and calcium ion channels, as well as through influences on mitochondrial function and metabolic pathways.[32] However, the clinical relevance of these mechanisms requires further substantiation. HSN (**6**) has also been reported to protect cardiomyocytes from hypoxia-induced apoptosis by modulating Bcl-2 family proteins and caspase-dependent signaling pathways, thereby limiting cellular destruction and enhancing myocardial function. Additional studies suggest that HSN (**6**) may attenuate the progression of acute myocardial infarction by suppressing lipid peroxidation through upregulation of antioxidant enzymes, ultimately reducing cardiomyocyte necrosis and lowering injury biomarkers such as lactate dehydrogenase (LDH) and reactive oxygen species (ROS).[26,174] Yohimbine (**8**) similarly exhibits cardioprotective properties, as evidenced by its ability to inhibit lipopolysaccharide (LPS)-induced myocardial apoptosis through significant reductions in TNF-α, caspase-3/7, and IL-1β levels.[175]

5.4 Analgesia

M. speciosa is recognized for its diverse array of corynanthe-type alkaloids. Watanabe *et al.*[153,176] demonstrated that corynantheidine selectively binds to μ-opioid receptors (MORs) in receptor-binding assays. Pharmacological studies have potentially shown that mitragynine (**1**) possesses analgesic properties across both *in vivo* and *in vitro* models. However, mitragynine (**1**) displays lower potency compared to its more active metabolites, mitragynine pseudoindoxyl and 7-hydroxymitragynine—the latter a minor constituent of *M. speciosa* that exhibits markedly stronger activity at opioid receptors. Specifically, 7-hydroxymitragynine displays approximately 13-fold higher potency than morphine and 46-fold higher potency than mitragynine (**1**). Both mitragynine (**1**) and 7-hydroxymitragynine show robust pharmacological profiles, underscoring their promise as novel opioid-targeted analgesics.[177] Furthermore, (3*S*,4*S*,15*S*,20*R*)-antirhine N_4-oxide has demonstrated mild analgesic effects in the mouse hot-plate assay at a dosage of 20 mg kg^{-1} administered intraperitoneally.[178] Notably, the analgesic actions of these compounds appear dose-dependent and are predominantly mediated *via* opioid pathways, as evidenced by naloxone-induced reversal. However, an exclusive focus on receptor-specific mechanisms may overlook important off-target interactions, potentially oversimplifying their pharmacological profiles.[179]

5.5 Anti-cancer

Luesch *et al.* reported that yohimbine (**8**) and its derivatives antagonize GPCR-mediated oncogenic signaling pathways.[119] Consistent with this, yohimbine (**8**) has been shown to exert pro-apoptotic effects in PC-2 and PC-3 pancreatic cancer cell lines.[180] Several synthesized yohimbine analogs also demonstrated selective cytotoxicity toward human pancreatic (PATU-8988) and gastric (SGC7901) cancer cells, while exhibiting comparatively lower toxicity in normal gastric mucosal cells (GES1).[181] These antitumor effects have been tent attributed to the inhibition of GPCR-driven cAMP/PKA signaling by yohimbine (**8**), leading to suppressed cancer cell proliferation.[182] HSN (**6**) has likewise shown potent cytotoxicity across multiple human breast cancer cell lines, including MCF-7, MDA-MB-231, MCF-10A, BT474, and MDA-MB-453.[25,156,157,183] Hayakawa *et al.*[157] demonstrated that HSN (**6**) triggers programmed cell death MDA-MB-231 cells by reducing the Bcl-2/Bax ratio, promoting mitochondrial permeability transition pore opening, inducing cytochrome c release, and activating caspases-9 and caspases-3. Conversely, Li *et al.*[184] found that HSN (**6**) inhibited Jurkat clone E6-1 cell death through compensatory upregulation of Bcl-2. In an A549 xenograft mouse model, Zhou *et al.*[185] showed that HSN (**6**) inhibits tumor development and promotes apoptosis through ROCK1/PTEN/PI3K/Akt/GSK3 signaling. Zhan *et al.*[186] showed that ajmalicine (**7**) demonstrates antitumor potential by inducing pyroptosis in H22 cells by elevating intracellular ROS, increasing pyroptosis rates and upregulating inflammatory mediators such as TNF-α, IL-1β, and IL-6. *In vivo*, ajmalicine (**7**) inhibited tumor progression and was shown to act through a noncanonical caspase-3/GSDME-dependent pyroptotic pathway. Collectively, although these indole alkaloids display promising anticancer activity across preclinical systems, their mechanisms remain incompletely resolved and appear highly context-dependent. Further work is necessary to define their selectivity, efficacy, and safety before their therapeutic potential can be fully established.

5.6 Others

Yohimbine (**8**) is generally well-tolerated in clinical populations with psychogenic erectile dysfunction, with studies reporting minimal adverse events.[187] In patients with organic erectile dysfunction, dose-escalation testing suggested enhanced efficacy upon doubling the dose, without significant adverse effects, abnormal cardiovascular responses, or notable changes in blood pressure.[188] In animal studies, yohimbine (**8**) increased sexual arousal and mating behavior in male rats without altering testosterone, follicle-stimulating hormone, or luteinizing hormone levels. Consistent with these findings, isolated rat corpus cavernosum preparations showed a dose-dependent relaxant effect.[189] HSN (**6**) exhibits notable antiviral activity.[190] It inhibits all four dengue virus serotypes by disrupting viral assembly, budding, or release, while leaving translation and replication largely unaffected. Its antiviral effects may also involve modulation of cellular calcium homeostasis.[191] HSN (**6**) has further demonstrated inhibitory activity against influenza A strains (H_3N_2 subtype).[192] Yohimbine (**8**) has also been

Table 2 Biological activity of corynanthe and related alkaloids

Compound name	Biological activity	Efficacy	References
Mitragynine	Opioid receptor	0.1–3.0 mg kg^{-1} in rats, *in vivo*	151
	Analgesic	300 nM–10 μM in guinea-pig, *in vivo*	152
	Antinociceptive	10 μg, i.c.v. in mouse, *in vivo*	153
	Antiinflammatory	10–20 μg ml^{-1}, RAW264.7 cells, *in vitro*	154
Corynanthine	Antileishmanial	$IC_{50} = 23.4 \pm 5.4$ μM in *L. major*, *in vitro*	13
	Cytotoxicity	$IC_{50} = 186 \pm 1$ μM in KB-3-1 cells, $IC_{50} = 214 \pm 26$ μM in KB-VI cells, *in vitro*	
Corynantheidine	Antileishmanial	$IC_{50} = 2.81 \pm 0.4$ μM in *L. major*, *in vitro*	
	Antimalarial	$IC_{50} = 41.1 \pm 2.5$ μM in *P. falciparum*, *in vitro*	
	Cytotoxicity	$IC_{50} = 80 \pm 8$ μM in KB-3-1 cells, $IC_{50} = 80 \pm 5$ μM in KB-VI cells, *in vitro*	
Corynantheine	Antileishmanial	$IC_{50} = 1.12 \pm 0.4$ μM in *L. major*, *in vitro*	
	Antimalarial	$IC_{50} = 81.1 \pm 1.6$ μM in *P. falciparum*, *in vitro*	
	Cytotoxicity	$IC_{50} = 140 \pm 11$ μM in KB-3-1 cells, $IC_{50} = 144 \pm 4$ μM in KB-VI cells, *in vitro*	
Dihydrocorynantheine	Antileishmanial	$IC_{50} = 1.65 \pm 0.3$ μM in *L. major*, *in vitro*	
	Antimalarial	$IC_{50} = 66.4 \pm 6.5$ μM in *P. falciparum*, *in vitro*	
	Cytotoxicity	$IC_{50} = 161 \pm 19$ μM in KB-3-1 cells, $IC_{50} = 158 \pm 15$ μM in KB-VI cells, *in vitro*	
Tetrahydroalstonine	Neuro-protection	10 μM in SK-N-MC cells, *in vitro*	155
Hirsutine	Cardioprotective activity	5–20 mg kg^{-1} in rats, *in vivo*	26
	Cytotoxicity	6.2–80 μM in NCI-H1299, MCF-10A, MCF-7, MDA-MB-231, and 4T1 cells, *in vitro*	25, 156 and 157
	Inflammation	35–140 mg kg^{-1}, b.w. in rats, *in vivo*	158
	Antihypertensive	$IC_{50} = 1.129 \times 10^{-9} \pm 0.5025$ μM, in rats, *in vivo*	159
Ajmalicine	Antileishmanial	$IC_{50} = 0.57 \pm 0.1$ μM in *L. major*, *in vitro*	13
	Nicotinic receptor antagonism	$IC_{50} = 72.3 \pm 22.5$ μM, *in vitro*	160
Yohimbine	Anticancer	$IC_{50} = 25.5$ μM in MCF-7, *in vitro* cells, $IC_{50} = 22.6$ μM in SWS80 cells, and $IC_{50} = 26.0$ μM in A549 cells, *in vitro*	43
	Anti-inflammatory	2–8 mg kg^{-1} in rats, *in vivo*	161
	Adrenoceptor α_2 inhibition	KI = 0.88 nM (α2C), *in vitro*	29
Rauwolscine	α_2-Adrenoceptor antagonist	2.24 mg kg^{-1} in rats, *in vivo*	162
	Antileishmanial	$IC_{50} = 23.8 \pm 2.6$ μM in *L. major*, *in vitro*	13
	Cytotoxic	$IC_{50} = 200 \pm 23$ μM in KB-3-1 cells, $IC_{50} = 263 \pm 12$ μM in KB-VI cells, *in vitro*	
Reserpine	Antileishmanial	$IC_{50} = 16.4 \pm 2.3$ μM in *L. major*, *in vitro*	
	Antimalarial	$IC_{50} = 8.1 \pm 0.4$ μM in *P. falciparum*, *in vitro*	
	Hypotensive	0.5 mg day^{-1} (clinical trials)	31
Rhynchophylline	Anti-inflammatory	0.3–30 μM in mouse N9 microglial cells, *in vitro*	163
	Neuro-protection	50 mg kg^{-1} in mouse, *in vivo*	164
Ajmaline	Antimalarial	$IC_{50} = 121 \pm 9$ μM in *P. falciparum*, *in vitro*	13
	Anti-arrhythmia	$IC_{50} = 1.70$ μM (Kv1.5)/2.66 μM (Kv4.3) in CHO cells, *in vitro*	165

investigated in metabolic disorders. In high-fat diet induced obese rats, it produced significant weight loss and appetite suppression accompanied by improvements in lipid and carbohydrate metabolism, with no major adverse effects reported.[193] Sapa *et al.*[194] additionally showed that yohimbine (**8**) ameliorates dysregulated lipid and carbohydrate homeostasis in conditions of leptin deficiency and impaired α_2- and β3-adrenergic receptor function.

6 Conclusion and future prospect

Despite substantial progress in elucidating the biosynthetic pathways of selected corynanthe alkaloids, critical gaps remain in the functional annotation of several rate-limiting enzymes and short-lived intermediates. These unresolved steps hinder efforts to optimize microbial chassis systems for scalable industrial production. Traditional chemical routes, although historically important, typically deliver modest yields due to multistep synthetic sequences, the thermodynamic lability of advanced intermediates, and competing side reactions. The inherent architectural complexity of corynanthe alkaloids—including their polycyclic scaffolds and multiple contiguous stereocenters—further imposes strict constraints on stereochemical fidelity and regioselective control. As a result, current methodologies frequently rely on protective-group manipulations to suppress undesired reactivity, which in turn inflate synthetic burden and production costs. Subsequent deprotection steps may also compromise product integrity, reducing overall yield or altering molecular structure.

Corynanthe alkaloids have garnered wide interest due to their anti-inflammatory, analgesic, and neuroleptic properties. However, the presence of multiple stereogenic centers, such as C3 and C15/C16, complicates structural optimization and hinders mechanistic elucidation of their pharmacological activities. A clearer understanding of structure–activity relationships is therefore essential. The naturally low abundance of these alkaloids in plant sources further constrains their extraction and large-scale utilization, underscoring the need for alternative production strategies such as synthetic biology and metabolic engineering. Recent methodological innovations have begun to address these challenges. Beniddir *et al.*[9] introduced a "spectral skeleton" correlation strategy that integrates Tanimoto structural similarity metrics with enhanced cosine similarity scoring to reveal conserved mass-spectral features of ajmalicine and corynantheane spirooxindoles. This approach offers a powerful means for rapid identification of key intermediates and biosynthetic products. Tools such as SpectraToQueries and MassQL further enable the conversion of characteristic mass-spectral signatures of specific scaffolds (*e.g.*, corynantheane) into machine-readable queries, facilitating rapid verification of target skeletons and substantially improving synthetic efficiency. The broader "Spectral Signature" framework allows chemists to extract defining mass-spectral motifs of complex natural-product backbones (*e.g.*, corynanthe dimers) and retro-design synthetic routes that guarantee construction of essential structural fragments, thereby advancing precision-oriented synthesis. Moreover, the successful *de novo* biosynthesis of MIAs such as vinblastine and ajmaline in heterologous hosts has strengthened confidence in the feasibility of producing high-value MIAs *via* engineered systems. These achievements lay a foundation for generating natural products and analogs with enhanced bioactivity and for the rational design of safer, more effective therapeutic agents.

7 Author contributions

Chenxu Liu: Writing – review & editing, writing – original draft, visualization, investigation, conceptualization. Mengqi Tong: writing – review & editing, conceptualization. Kouharu Otsuki: writing – review & editing, conceptualization. Wei Li: writing – review & editing, conceptualization. Feng Feng: writing – review & editing, supervision, conceptualization. Jie Zhang: conceptualization, writing – review & editing, supervision, project administration.

8 Conflicts of interest

All authors declare that they have no competing interests.

9 Data availability

No primary research results, software or code have been included and no new data were generated or analysed as part of this review.

10 Acknowledgments

This work was supported by grants from General Program of the National Natural Science Foundation of China (No. [82574277]).

11 References

1 S. Zhou, Y. Ma, Y. Shang, X. Qi, S. Huang and J. Li, *Life Metab.*, 2022, **1**, 109–121.
2 T. Kouamé, A. T. Okpekon, N. F. Bony, A. D. N'Tamon, J. F. Gallard, S. Rharrabti, K. Leblanc, E. Mouray, P. Grellier, P. Champy, M. A. Beniddir and P. Le Pogam, *Molecules*, 2020, **25**, 2654.
3 A. Mauger, M. Jarret, C. Kouklovsky, E. Poupon, L. Evanno and G. Vincent, *Nat. Prod. Rep.*, 2021, **38**, 1852–1886.
4 A. C. Ramos-Valdivia and C. M. Cerda-García-Rojas, *Curr. Opin. Plant Biol.*, 2024, **82**, 102648.
5 H. Takayama, H. Ishikawa, M. Kurihara, M. Kitajima, N. Aimi, D. Ponglux, F. Koyama, K. Matsumoto, T. Moriyama, L. T. Yamamoto, K. Watanabe, T. Murayama and S. Horie, *J. Med. Chem.*, 2002, **45**, 1949–1956.
6 Y. Nam, A. T. Tam, E. R. Miller and K. A. Scheidt, *J. Am. Chem. Soc.*, 2024, **146**, 118–124.
7 J. Li, J. X. Li, H. Jiang, M. Li, L. Chen, Y. Y. Wang, L. Wang, N. Zhang, H. Z. Guo and K. L. Ma, *Phytochemistry*, 2023, **213**, 113786.
8 A. E. Fox Ramos, P. Le Pogam, C. Fox Alcover, E. Otogo N'Nang, G. Cauchie, H. Hazni, K. Awang, D. Bréard, A. M. Echavarren, M. Frédérich, T. Gaslonde, M. Girardot, R. Grougnet, M. S. Kirillova, M. Kritsanida, C. Lémus, A. M. Le Ray, G. Lewin, M. Litaudon, L. Mambu, S. Michel, F. M. Miloserdov, M. E. Muratore, P. Richomme-Peniguel, F. Roussi, L. Evanno, E. Poupon, P. Champy and M. A. Beniddir, *Sci. Data*, 2019, **6**, 15.
9 S. Szwarc, A. Rutz, K. Lee, Y. Mejri, O. Bonnet, H. Hazni, A. Jagora, R. B. Mbeng Obame, J. K. Noh, E. Otogo N'Nang, S. C. Alaribe, K. Awang, G. Bernadat, Y. H. Choi, V. Courdavault, M. Frederich, T. Gaslonde, F. Huber, T. S. Kam, Y. Y. Low, E. Poupon, J. J. J. van der Hooft, K. B. Kang, P. Le Pogam and M. A. Beniddir, *J. Cheminf.*, 2025, **17**, 62.
10 S. H. Dong, Z. K. Duan, M. Bai, X. X. Huang and S. J. Song, *TrAC, Trends Anal. Chem.*, 2024, **175**, 117711.
11 T. M. D. Ebbels, J. J. J. van der Hooft, H. Chatelaine, C. Broeckling, N. Zamboni, S. Hassoun and E. A. Mathé, *Curr. Opin. Chem. Biol.*, 2023, **74**, 102288.
12 A. Rutz, M. Sorokina, J. Galgonek, D. Mietchen, E. Willighagen, A. Gaudry, J. G. Graham, R. Stephan, R. Page, J. Vondrášek, C. Steinbeck, G. F. Pauli, J. L. Wolfender, J. Bisson and P. M. Allard, *eLife*, 2022, **11**, e70780.
13 D. Staerk, E. Lemmich, J. Christensen, A. Kharazmi, C. E. Olsen and J. W. Jaroszewski, *Planta Med.*, 2000, **66**, 531–536.
14 T. Dugé de Bernonville, I. Carqueijeiro, A. Lanoue, F. Lafontaine, P. Sánchez Bel, F. Liesecke, K. Musset, A. Oudin, G. Glévarec, O. Pichon, S. Besseau, M. Clastre,

B. St-Pierre, V. Flors, S. Maury, E. Huguet, S. E. O'Connor and V. Courdavault, *Sci. Rep.*, 2017, **7**, 40453.
15 G. M. Halpenny, *ACS Med. Chem. Lett.*, 2017, **8**, 897–899.
16 D. A. Todd, J. J. Kellogg, E. D. Wallace, M. Khin, L. Flores-Bocanegra, R. S. Tanna, S. McIntosh, H. A. Raja, T. N. Graf, S. E. Hemby, M. F. Paine, N. H. Oberlies and N. B. Cech, *Sci. Rep.*, 2020, **10**, 19158.
17 A. Banerji, P. L. Majumder and A. Chatterjee, *Phytochemistry*, 1970, **9**, 1491–1493.
18 R. Van Der Heijden, D. I. Jacobs, W. Snoeijer, D. Hallard and R. Verpoorte, *Curr. Med. Chem.*, 2004, **11**, 607–628.
19 J. F. Treimer and M. H. Zenk, *Phytochemistry*, 1978, **17**, 227–231.
20 R. Eckermann and T. Gaich, *Chem.–Eur. J.*, 2016, **22**, 5749–5755.
21 Y. M. Liao, J. Y. Wang, Y. Pan, X. Y. Zou, C. Q. Wang, Y. H. Peng, Y. L. Ao, M. F. Lam, X. S. Zhang, X. Q. Zhang, L. Shi and S. Q. Zhang, *Molecules*, 2023, **28**, 2370.
22 S. Malik, *Planta Med.*, 1984, **50**, 283.
23 D. Arbain, D. P. Putra and M. V. Sargent, *Planta Med.*, 1991, **57**, 396.
24 S. Horie, S. Yano, N. Aimi, S. Sakai and K. Watanabe, *Life Sci.*, 1992, **50**, 491–498.
25 C. Lou, K. Takahashi, T. Irimura, I. Saiki and Y. Hayakawa, *Int. J. Oncol.*, 2014, **45**, 2085–2091.
26 L. X. Wu, X. F. Gu, Y. C. Zhu and Y. Z. Zhu, *Eur. J. Pharmacol.*, 2011, **650**, 290–297.
27 K. Sugimura, S. Katsuki, R. Arai, H. Kamiya, T. Kawasaki, O. Iida, N. Kawahara, S. S. Shrestha, S. Dall'Acqua and T. Watanabe, *Fitoterapia*, 2024, **178**, 106132.
28 F. León, E. Habib, J. E. Adkins, E. B. Furr, C. R. McCurdy and S. J. Cutler, *Nat. Prod. Commun.*, 2009, **4**, 907–910.
29 H. B. Liu, Y. Peng, L. Q. Huang, J. Xu and P. G. Xiao, *J. Chem.*, 2013, **2013**, 9.
30 S. Surendran, R. Raju, P. Prasannan and A. Surendran, *Bot. Rev.*, 2021, **87**, 311–376.
31 S. D. Shamon and M. I. Perez, *Cochrane Database Syst. Rev.*, 2016, **12**, Cd007655.
32 M. M. Monasky, E. Micaglio, S. D'Imperio and C. Pappone, *Front. Cardiovasc. Med.*, 2021, **8**, 782596.
33 T. Kang, Y. Murakami, H. Takayama, M. Kitajima, N. Aimi, H. Watanabe and K. Matsumoto, *Life Sci.*, 2004, **76**, 331–343.
34 J. S. Shi, J. X. Yu, X. P. Chen and R. X. Xu, *Acta Pharmacol. Sin.*, 2003, **24**, 97–101.
35 Y. P. Liu, P. K. Ju, J. T. Long, L. Lai, W. H. Zhao, C. Zhang, Z. J. Zhang and Y. H. Fu, *Nat. Prod. Res.*, 2018, **32**, 2922–2927.
36 S. Y. Liew, C. Y. Looi, M. Paydar, F. K. Cheah, K. H. Leong, W. F. Wong, M. R. Mustafa, M. Litaudon and K. Awang, *PLoS One*, 2014, **9**, e87286.
37 H. Jiang, Y. B. Liu, Y. Li, L. Li, S. G. Ma, J. Qu and S. S. Yu, *Tetrahedron*, 2016, **72**, 1276–1284.
38 J. Zhang, H. Li, Y. Li, Z. W. Li, C. C. Sang, M. H. Gao, D. M. Zhang, X. Q. Zhang and W. C. Ye, *Chin. J. Nat. Med.*, 2019, **17**, 918–923.
39 M. F. Bao, C. X. Zeng, Y. P. Liu, B. J. Zhang, L. Ni, X. D. Luo and X. H. Cai, *J. Nat. Prod.*, 2017, **80**, 790–797.
40 N. P. Li, M. Liu, X. J. Huang, X. Y. Gong, W. Zhang, M. J. Cheng, W. C. Ye and L. Wang, *J. Org. Chem.*, 2018, **83**, 5707–5714.
41 A. N. Bitombo, A. A. A. Zintchem, A. D. T. Atchadé, N. Mbabi Nyemeck Ii, D. S. N. Bikobo, D. E. Pegnyemb and C. G. Bochet, *Fitoterapia*, 2021, **153**, 104941.
42 G. Q. Zhan, R. K. Miao, F. X. Zhang, G. Chang, L. Zhang, X. X. Zhang, H. Zhang and Z. J. Guo, *Bioorg. Chem.*, 2020, **102**, 104136.
43 G. Q. Zhan, R. K. Miao, F. X. Zhang, X. B. Wang, X. X. Zhang and Z. J. Guo, *Chem. Biodiversity*, 2020, **17**, e2000647.
44 H. Q. Pan, W. Z. Yang, D. Zhao, C. Luo, C. L. Yao, X. J. Shi, Y. B. Zhang, S. Y. Li, Y. Bi, Z. Wang, S. Yao, W. Y. Wu and D. A. Guo, *Fitoterapia*, 2017, **116**, 85–92.
45 Q. Guo, X. L. Si, Y. T. Shi, H. S. Yang, X. Y. Liu, H. Liang, P. F. Tu and Q. Y. Zhang, *J. Nat. Prod.*, 2019, **82**, 3288–3301.
46 S. Tan, J. Lim, Y. Low, K. Sim, S. Lim and T. Kam, *J. Nat. Prod.*, 2014, **77**, 2068–2080.
47 L. Liu, Y. Chen, X. Qin, B. Wang, Q. Jin, Y. Liu and X. Luo, *Fitoterapia*, 2015, **105**, 160–164.
48 P. Amelia, A. E. Nugroho, Y. Hirasawa, T. Kaneda, T. Tougan, T. Horii and H. Morita, *J. Nat. Med.*, 2019, **73**, 820–825.
49 L. Pan, C. Terrazas, U. M. Acuña, T. N. Ninh, H. Chai, E. J. Carcache de Blanco, D. D. Soejarto, A. R. Satoskar and A. D. Kinghorn, *Phytochem. Lett.*, 2014, **10**, liv–lix.
50 J. S. Yeap, C. H. Tan, K. T. Yong, K. H. Lim, S. H. Lim, Y. Y. Low and T. S. Kam, *Phytochemistry*, 2020, **176**, 112391.
51 J. S. Yeap, S. Navanesan, K. S. Sim, K. T. Yong, S. Gurusamy, S. H. Lim, Y. Y. Low and T. S. Kam, *J. Nat. Prod.*, 2018, **81**, 1266–1277.
52 A. E. Nugroho, M. Sugai, Y. Hirasawa, T. Hosoya, K. Awang, A. H. Hadi, W. Ekasari, A. Widyawaruyanti and H. Morita, *Bioorg. Med. Chem. Lett.*, 2011, **21**, 3417–3419.
53 K. Zaima, I. Koga, N. Iwasawa, T. Hosoya, Y. Hirasawa, T. Kaneda, I. S. Ismail, N. H. Lajis and H. Morita, *J. Nat. Med.*, 2013, **67**, 9–16.
54 Y. Wu, M. Kitajima, N. Kogure, R. Zhang and H. Takayama, *Tetrahedron Lett.*, 2008, **49**, 5935–5938.
55 R. N. Iyer, D. Favela, G. Zhang and D. E. Olson, *Nat. Prod. Rep.*, 2021, **38**, 307–329.
56 X. Tong, B. Shi, Q. Liu, Y. Huo and C. Xia, *Org. Biomol. Chem.*, 2019, **17**, 8062–8066.
57 L. V. Méteignier, S. Szwarc, P. Barunava, M. Durand, D. L. Zamar, C. Birer Williams, N. Gautron, C. Dutilleul, K. Koudounas, E. Lezin, T. Perrot, A. Oudin, S. Pateyron, E. Delannoy, V. Brunaud, A. Lanoue, B. H. Abbasi, B. St-Pierre, M. K. Jensen, N. Papon, C. Sun, P. Le Pogam, L. Yuan, M. A. Beniddir, S. Besseau and V. Courdavault, *Plant Physiol. Biochem.*, 2025, **219**, 109363.
58 V. Salim, F. Yu, J. Altarejos and V. De Luca, *Plant J.*, 2013, **76**, 754–765.
59 A. Böttger, U. Vothknecht, C. Bolle and A. Wolf, in *Lessons on Caffeine, Cannabis & Co: Plant-derived Drugs and their Interaction with Human Receptors*, ed. A. Böttger, U.

Vothknecht, C. Bolle and A. Wolf, Springer International Publishing, Cham, 2018, pp. 153–170.
60 S. W. Wu, M. Q. Yang and Y. L. Xiao, *Chin. J. Org. Chem.*, 2018, **38**, 2243–2258.
61 D. Pressnitz, E. M. Fischereder, J. Pletz, C. Kofler, L. Hammerer, K. Hiebler, H. Lechner, N. Richter, E. Eger and W. Kroutil, *Angew Chem. Int. Ed. Engl.*, 2018, **57**, 10683–10687.
62 X. Zhu, X. Zeng, C. Sun and S. Chen, *Front. Med.*, 2014, **8**, 285–293.
63 S. E. O'Connor and J. J. Maresh, *Nat. Prod. Rep.*, 2006, **23**, 532–547.
64 X. Y. Ma, J. Koepke, G. Fritzsch, R. Diem, T. M. Kutchan, H. Michel and J. Stöckigt, *Biochim. Biophys. Acta, Proteins Proteomics*, 2004, **1702**, 121–124.
65 C. L. G. Santos, C. F. F. Angolini, K. O. G. Neves, E. V. Costa, A. D. L. de Souza, M. L. B. Pinheiro, H. H. F. Koolen and F. M. A. da Silva, *Rapid Commun. Mass Spectrom.*, 2020, **34**(3), e8683.
66 C. Langley, E. Tatsis, B. Hong, Y. Nakamura, C. Paetz, C. E. M. Stevenson, J. Basquin, D. M. Lawson, L. Caputi and S. E. O'Connor, *Angew Chem. Int. Ed. Engl.*, 2022, **61**, e202210934.
67 T. M. Kutchan, N. Hampp, F. Lottspeich, K. Beyreuther and M. H. Zenk, *FEBS Lett.*, 1988, **237**, 40–44.
68 T. D. McKnight, C. A. Roessner, R. Devagupta, A. I. Scott and C. L. Nessler, *Nucleic Acids Res.*, 1990, **18**, 4939.
69 G. Pasquali, O. J. Goddijn, A. de Waal, R. Verpoorte, R. A. Schilperoort, J. H. Hoge and J. Memelink, *Plant Mol. Biol.*, 1992, **18**, 1121–1131.
70 Y. Yamazaki, H. Sudo, M. Yamazaki, N. Aimi and K. Saito, *Plant Cell Physiol.*, 2003, **44**, 395–403.
71 S. Brown, M. Clastre, V. Courdavault and S. E. O'Connor, *Proc. Natl. Acad. Sci. U. S. A.*, 2015, **112**, 3205–3210.
72 E. Fischereder, D. Pressnitz, W. Kroutil and S. Lutz, *Bioorg. Med. Chem.*, 2014, **22**, 5633–5637.
73 X. Ma, S. Panjikar, J. Koepke, E. Loris and J. Stöckigt, *Plant Cell*, 2006, **18**, 907–920.
74 M. Yang, B. Yao and R. Lin, *Biomolecules*, 2022, **12**, 1790.
75 T. J. C. Luijendijk, L. H. Stevens and R. Verpoorte, *Plant Physiol. Biochem.*, 1998, **36**, 419–425.
76 A. A. Qureshi and A. I. Scott, *Chem. Commun.*, 1968, 945–946.
77 C. X. Jiang, J. X. Yu, X. Fei, X. J. Pan, N. N. Zhu, C. L. Lin, D. Zhou, H. R. Zhu, Y. Qi and Z. G. Wu, *Int. J. Biol. Macromol.*, 2023, **226**, 1360–1373.
78 P. Bernhardt, E. McCoy and S. E. O'Connor, *Chem. Biol.*, 2007, **14**, 888–897.
79 N. Cao and C. H. Wang, *Chin. J. Nat. Med.*, 2021, **19**, 591–607.
80 P. Chakraborty, A. Biswas, S. Dey, T. Bhattacharjee and S. Chakrabarty, *J. Xenobiot.*, 2023, **13**, 402–423.
81 Z. Liu, J. Pang, Y. Li, D. Wei, J. Yang, X. Wang and Y. Luo, *Physiol. Plant.*, 2024, **176**, e14515.
82 D. Williams and V. De Luca, *Phytochem. Rev.*, 2023, **22**, 309–338.
83 J. Liang, T. An, J. X. Zhu, S. Chen, J. H. Zhu, R. J. Peters, R. Yu and J. Zi, *J. Nat. Prod.*, 2021, **84**, 2709–2716.
84 D. Ratnadewi, in *Alkaloids - Alternatives in Synthesis, Modification and Application*, ed. V. Georgiev and A. Pavlov, IntechOpen, Rijeka, 2017, DOI: 10.5772/66288.
85 T. T. Dang, J. Franke, I. S. T. Carqueijeiro, C. Langley, V. Courdavault and S. E. O'Connor, *Nat. Chem. Biol.*, 2018, **14**, 760–763.
86 B. Hong, D. Grzech, L. Caputi, P. Sonawane, C. E. R. López, M. O. Kamileen, N. J. Hernández Lozada, V. Grabe and S. E. O'Connor, *Nature*, 2022, **607**, 617–622.
87 E. C. Tatsis, I. Carqueijeiro, T. Dugé de Bernonville, J. Franke, T.-T. T. Dang, A. Oudin, A. Lanoue, F. Lafontaine, A. K. Stavrinides, M. Clastre, V. Courdavault and S. E. O'Connor, *Nat. Commun.*, 2017, **8**, 316.
88 Z. Wang, Y. R. Xiao, S. Wu, J. H. Chen, A. Li and E. C. Tatsis, *Chem. Sci.*, 2022, **13**, 12389–12395.
89 S. C. Farrow, M. O. Kamileen, L. Caputi, K. Bussey, J. E. A. Mundy, R. C. McAtee, C. R. J. Stephenson and S. E. O'Connor, *J. Am. Chem. Soc.*, 2019, **141**, 12979–12983.
90 L. Caputi, J. Franke, S. C. Farrow, K. Chung, R. M. E. Payne, T.-D. Nguyen, T.-T. T. Dang, I. Soares Teto Carqueijeiro, K. Koudounas, T. Dugé de Bernonville, B. Ameyaw, D. M. Jones, I. J. C. Vieira, V. Courdavault and S. E. O'Connor, *Science*, 2018, **360**, 1235–1239.
91 Y. Qu, M. Easson, R. Simionescu, J. Hajicek, A. M. K. Thamm, V. Salim and V. De Luca, *Proc. Natl. Acad. Sci. U. S. A.*, 2018, **115**, 3180–3185.
92 T. T. Dang, J. Franke, E. Tatsis and S. E. O'Connor, *Angew Chem. Int. Ed. Engl.*, 2017, **56**, 9440–9444.
93 H. Falkenhagen and J. Stöckigt, *Z. Naturforsch., C*, 1995, **50**, 45–53.
94 D. Schmidt and J. Stöckigt, *Planta Med.*, 1995, **61**, 254–258.
95 K. Chang, M. Chen, L. Zeng, X. Lan, Q. Wang and Z. H. Liao, *Russ. J. Plant Physiol.*, 2014, **61**, 136–140.
96 T. Liu, Y. Gou, B. Zhang, R. Gao, C. Dong, M. Qi, L. Jiang, X. Ding, C. Li and J. Lian, *Biotechnol. Bioeng.*, 2022, **119**, 1314–1326.
97 G. Dai, Q. Shen, Y. Zhang and X. Bian, *J. Fungi*, 2022, **8**, 320.
98 J. Q. Cao, J. X. Zhong, F. Li and Y. D. Jiang, *J. Am. Chem. Soc.*, 2025, **147**, 25233–25241.
99 T. A. Nguyen, D. Grzech, K. Chung, Z. Xia, T. D. Nguyen and T. T. Dang, *Front. Plant Sci.*, 2023, **14**, 1125158.
100 M. O. Kamileen, B. Hong, K. Gase, M. Kunert, L. Caputi, B. R. Lichman and S. E. O'Connor, *Angew Chem. Int. Ed. Engl.*, 2025, **64**, e202501323.
101 F. Ferreres, D. M. Pereira, P. Valentão, J. M. Oliveira, J. Faria, L. Gaspar, M. Sottomayor and P. B. Andrade, *J. Pharm. Biomed. Anal.*, 2010, **51**, 65–69.
102 W. T. Jeong and H. B. Lim, *J. Chromatogr., B: Anal. Technol. Biomed. Life Sci.*, 2018, **1080**, 27–36.
103 F. Krengel, M. V. Mijangos, M. Reyes-Lezama and R. Reyes-Chilpa, *Chem. Biodivers.*, 2019, **16**, e1900175.
104 H. Ishikawa, D. A. Colby, S. Seto, P. Va, A. Tam, H. Kakei, T. J. Rayl, I. Hwang and D. L. Boger, *J. Am. Chem. Soc.*, 2009, **131**, 4904–4916.

105 A. Verma, I. Laakso, T. Seppänen-Laakso, A. Huhtikangas and M. L. Riekkola, *Molecules*, 2007, **12**, 1307–1315.
106 J. Zhang, L. G. Hansen, O. Gudich, K. Viehrig, L. M. M. Lassen, L. Schrübbers, K. B. Adhikari, P. Rubaszka, E. Carrasquer-Alvarez, L. Chen, V. D'Ambrosio, B. Lehka, A. K. Haidar, S. Nallapareddy, K. Giannakou, M. Laloux, D. Arsovska, M. A. K. Jørgensen, L. J. G. Chan, M. Kristensen, H. B. Christensen, S. Sudarsan, E. A. Stander, E. Baidoo, C. J. Petzold, T. Wulff, S. E. O'Connor, V. Courdavault, M. K. Jensen and J. D. Keasling, *Nature*, 2022, **609**, 341–347.
107 P. Cázares Flores, D. Levac and V. De Luca, *Plant J.*, 2016, **87**, 335–342.
108 J. Guo, D. Gao, J. Lian and Y. Qu, *Nat. Commun.*, 2024, **15**, 457.
109 A. Stavrinides, E. C. Tatsis, L. Caputi, E. Foureau, C. E. M. Stevenson, D. M. Lawson, V. Courdavault and S. E. O'Connor, *Nat. Commun.*, 2016, **7**, 12116.
110 E. A. Stander, B. Lehka, I. Carqueijeiro, C. Cuello, F. G. Hansson, H. J. Jansen, T. Dugé De Bernonville, C. Birer Williams, V. Vergès, E. Lezin, M. Lorensen, T. T. Dang, A. Oudin, A. Lanoue, M. Durand, N. Giglioli-Guivarc'h, C. Janfelt, N. Papon, R. P. Dirks, E. O'Connor S, M. K. Jensen, S. Besseau and V. Courdavault, *Commun. Biol.*, 2023, **6**, 1197.
111 C. Schotte, Y. D. Jiang, D. Grzech, T.-T. T. Dang, L. C. Laforest, F. León, M. Mottinelli, S. S. Nadakuduti, C. R. McCurdy and S. E. O'Connor, *J. Am. Chem. Soc.*, 2023, **145**, 4957–4963.
112 F. Trenti, K. Yamamoto, B. Hong, C. Paetz, Y. Nakamura and S. E. O'Connor, *Org. Lett.*, 2021, **23**, 1793–1797.
113 K. Kim, M. Shahsavarani, J. J. O. Garza-García, J. E. Carlisle, J. Guo, V. De Luca and Y. Qu, *New Phytol.*, 2023, **240**, 757–769.
114 Q. Pan, N. R. Mustafa, K. Tang, Y. H. Choi and R. Verpoorte, *Phytochem. Rev.*, 2016, **15**, 221–250.
115 D. J. Newman and G. M. Cragg, *J. Nat. Prod.*, 2020, **83**, 770–803.
116 K. A. Scott, N. Ropek, B. Melillo, S. L. Schreiber, B. F. Cravatt and E. V. Vinogradova, *Curr. Res. Chem. Biol.*, 2022, **2**, 100028.
117 S. B. Jones, B. Simmons, A. Mastracchio and D. W. MacMillan, *Nature*, 2011, **475**, 183–188.
118 X. B. Wang, D. L. Xia, W. F. Qin, R. J. Zhou, X. H. Zhou, Q. L. Zhou, W. T. Liu, X. Dai, H. J. Wang, S. Q. Wang, L. Tan, D. Zhang, H. Song, X. Y. Liu and Y. Qin, *Chem*, 2017, **2**, 803–816.
119 N. G. Paciaroni, V. M. Norwood, R. Ratnayake, H. Luesch and R. W. Huigens, *Bioorg. Med. Chem.*, 2020, **28**, 115546.
120 S. Majhi and D. Das, *Tetrahedron*, 2020, **78**, 131801.
121 H. Gotoh, K. K. Duncan, W. M. Robertson and D. L. Boger, *ACS Med. Chem. Lett.*, 2011, **2**, 948–952.
122 J. E. Sears and D. L. Boger, *Acc. Chem. Res.*, 2015, **48**, 653–662.
123 R. T. Brown, M. F. Jones and M. Wingfield, *J. Chem. Soc. Chem. Commun.*, 1984, 847–848.
124 S. Yu, O. M. Berner and J. M. Cook, *J. Am. Chem. Soc.*, 2000, **122**, 7827–7828.
125 J. Ma, W. Yin, H. Zhou and J. M. Cook, *Org. Lett.*, 2007, **9**, 3491–3494.
126 A. Deiters, M. Pettersson and S. F. Martin, *J. Org. Chem.*, 2006, **71**, 6547–6561.
127 T. Mizuno, Y. Oonishi, M. Takimoto and Y. Sato, *Eur. J. Org Chem.*, 2011, **2011**, 2606–2609.
128 X. F. Sun and D. W. Ma, *Chem.–Asian J.*, 2011, **6**, 2158–2165.
129 N. Ūdris, R. Ločmele, J. Pelšs, A. Ture, G. Sakaine, A. Kinēns and G. Smits, *Org. Chem. Front.*, 2025, **12**, 1945–1950.
130 T. Liu, Z. Huang, S. Cheng, W. Chen, X. Yang and H. Zhang, *Org. Lett.*, 2024, **26**, 8803–8809.
131 P. Angyal, K. Hegedüs, B. B. Mészáros, J. Daru, Á. Dudás, A. R. Galambos, N. Essmat, M. Al-Khrasani, S. Varga and T. Soós, *Angew. Chem., Int. Ed.*, 2023, **62**, e202303700.
132 D. J. Mergott, S. J. Zuend and E. N. Jacobsen, *Org. Lett.*, 2008, **10**, 745–748.
133 B. Herlé, M. J. Wanner, J. H. van Maarseveen and H. Hiemstra, *J. Org. Chem.*, 2011, **76**, 8907–8912.
134 Z. Q. Wang, K. Kaneda, Z. L. Fang and S. F. Martin, *Tetrahedron Lett.*, 2012, **53**, 477–479.
135 R. Riva, L. Banfi, B. Danieli, G. Guanti, G. Lesma and G. Palmisano, *J. Chem. Soc. Chem. Commun.*, 1987, 299–300.
136 A. K. Ghosh and A. Sarkar, *Eur. J. Org. Chem.*, 2016, **2016**, 6001–6009.
137 Z. C. Girvin, P. P. Lampkin, X. Liu and S. H. Gellman, *Org. Lett.*, 2020, **22**, 4568–4573.
138 C. Xie, J. Luo, Y. Zhang, L. Zhu and R. Hong, *Org. Lett.*, 2017, **19**, 3592–3595.
139 E. R. Miller, M. T. Hovey and K. A. Scheidt, *J. Am. Chem. Soc.*, 2020, **142**, 2187–2192.
140 M. Tang, H. Lu and L. Zu, *Nat. Commun.*, 2024, **15**, 941.
141 N. S. Rajapaksa, M. A. McGowan, M. Rienzo and E. N. Jacobsen, *Org. Lett.*, 2013, **15**, 706–709.
142 N. R. Jabir and S. Tabrez, *Curr. Pharm. Des.*, 2016, **22**, 940–946.
143 Y. Z. Liu, Y. X. Wang and C. L. Jiang, *Front. Hum. Neurosci.*, 2017, **11**, 316.
144 M. M. A. Neha and H. A. Khan, *Environ. Toxicol.*, 2017, **32**, 619–629.
145 F. Ou, Y. Huang, J. Sun, K. Su, Y. He, R. Zeng, D. Tang and G. Liao, *Inflammation*, 2021, **44**, 80–90.
146 G. G. Calhoon and K. M. Tye, *Nat. Neurosci.*, 2015, **18**, 1394–1404.
147 S. Kindler, S. Samietz, M. Houshmand, H. J. Grabe, O. Bernhardt, R. Biffar, T. Kocher, G. Meyer, H. Völzke, H. R. Metelmann and C. Schwahn, *J. Pain*, 2012, **13**, 1188–1197.
148 J. Lorenz, N. Schäfer, R. Bauer, Z. Jenei-Lanzl, R. H. Springorum and S. Grässel, *Osteoarthr. Cartil.*, 2016, **24**, 325–334.
149 R. G. Geetha and S. Ramachandran, *Pharmaceutics*, 2021, **13**, 1170.
150 Z. Zhou, Y. H. Su and X. E. Fa, *Life Sci.*, 2019, **223**, 137–145.
151 K. Yue, T. A. Kopajtic and J. L. Katz, *Psychopharmacology*, 2018, **235**, 2823–2829.

152 K. Matsumoto, L. T. Yamamoto, K. Watanabe, S. Yano, J. Shan, P. K. T. Pang, D. Ponglux, H. Takayama and S. Horie, *Life Sci.*, 2005, **78**, 187–194.
153 S. Thongpradichote, K. Matsumoto, M. Tohda, H. Takayama, N. Aimi, S. Sakai and H. Watanabe, *Life Sci.*, 1998, **62**, 1371–1378.
154 Z. Utar, M. I. A. Majid, M. I. Adenan, M. F. A. Jamil and T. M. Lan, *J. Ethnopharmacol.*, 2011, **136**, 75–82.
155 K. Chen and G. Yu, *Eur. J. Pharmacol.*, 2024, **962**, 176251.
156 Q. W. Huang, N. N. Zhai, T. Huang and D. M. Li, *Shengli Xuebao*, 2018, **70**, 40–46.
157 C. Lou, S. Yokoyama, I. Saiki and Y. Hayakawa, *Oncol. Rep.*, 2015, **33**, 2072–2076.
158 L. Z. Wu and X. M. Xiao, *Braz. J. Med. Biol. Res.*, 2019, **52**, e8273.
159 K. Zhu, S. N. Yang, F. F. Ma, X. F. Gu, Y. C. Zhu and Y. Z. Zhu, *PLoS One*, 2015, **10**, e0119477.
160 D. M. Pereira, F. Ferreres, J. M. Oliveira, L. Gaspar, J. Faria, P. Valentão, M. Sottomayor and P. B. Andrade, *Phytomedicine*, 2010, **17**, 646–652.
161 N. Sharma, R. Sistla and S. B. Andugulapati, *Phytomedicine*, 2024, **123**, 155182.
162 S. La Marca and R. W. Dunn, *Life Sci.*, 1994, **54**, Pl179–Pl184.
163 D. Yuan, B. Ma, J. Y. Yang, Y. Y. Xie, L. Wang, L. J. Zhang, Y. Kano and C. F. Wu, *Int. Immunopharmacol.*, 2009, **9**, 1549–1554.
164 A. K. Fu, K. W. Hung, H. Huang, S. Gu, Y. Shen, E. Y. Cheng, F. C. Ip, X. Huang, W. Y. Fu and N. Y. Ip, *Proc. Natl. Acad. Sci. U. S. A.*, 2014, **111**, 9959–9964.
165 F. Fischer, N. Vonderlin, E. Zitron, C. Seyler, D. Scherer, R. Becker, H. A. Katus and E. P. Scholz, *Naunyn-Schmiedebergs Arch Pharmacol*, 2013, **386**, 991–999.
166 L. Chen, Y. Huang, X. Yu, J. Lu, W. Jia, J. Song, L. Liu, Y. Wang, Y. Huang, J. Xie and M. Li, *Front. Pharmacol*, 2021, **12**, 642900.
167 X. Chen, J. Drew, W. Berney and W. Lei, *Cells*, 2021, **10**, 1309.
168 Y. F. Xian, Z. X. Lin, Q. Q. Mao, Z. Hu, M. Zhao, C. T. Che and S. P. Ip, *Evid. Based Complement. Alternat. Med.*, 2012, **2012**, 802625.
169 W. Yang, S. P. Ip, L. Liu, Y. F. Xian and Z. X. Lin, *Curr. Vasc. Pharmacol.*, 2020, **18**, 346–357.
170 P. Zeng, X. M. Wang, C. Y. Ye, H. F. Su and Q. Tian, *Int. J. Mol. Sci.*, 2021, **22**, 3612.
171 N. J. Chear, T. A. F. Ching-Ga, K. Y. Khaw, F. León, W. N. Tan, S. R. Yusof, C. R. McCurdy, V. Murugaiyah and S. Ramanathan, *Metabolites*, 2023, **13**, 390.
172 Y. Shimada, H. Goto, T. Itoh, I. Sakakibara, M. Kubo, H. Sasaki and K. Terasawa, *J. Pharm. Pharmacol.*, 1999, **51**, 715–722.
173 P. Nasa and D. Juneja, *Indian J. Crit. Care Med.*, 2016, **20**, 739–741.
174 W. Jiang, Y. Zhang, W. Zhang, X. Pan, J. Liu, Q. Chen and J. Chen, *Clin. Exp. Hypertens.*, 2023, **45**, 2192444.
175 Y. Y. Wang, H. M. Li, H. D. Wang, X. M. Peng, Y. P. Wang, D. X. Lu, R. B. Qi, C. F. Hu and J. W. Jiang, *Shock*, 2010, **35**, 322–328.
176 K. Matsumoto, M. Mizowaki, T. Suchitra, H. Takayama, S. Sakai, N. Aimi and H. Watanabe, *Life Sci.*, 1996, **59**, 1149–1155.
177 R. B. Raffa, J. R. Beckett, V. N. Brahmbhatt, T. M. Ebinger, C. A. Fabian, J. R. Nixon, S. T. Orlando, C. A. Rana, A. H. Tejani and R. J. Tomazic, *J. Med. Chem.*, 2013, **56**, 4840–4848.
178 J. Hua, Y. B. Liu, Y. Li, L. Li, S. G. Ma, J. Qu and S. S. Yu, *Tetrahedron*, 2016, **72**, 1276–1284.
179 H. Takayama, *Chem. Pharm. Bull.*, 2004, **52**, 916–928.
180 S. G. Shen, D. Zhang, H. T. Hu, J. H. Li, Z. Wang and Q. Y. Ma, *World J. Gastroenterol.*, 2008, **14**, 2358–2363.
181 H. Yang, M. Poznik, S. Tang, P. Xue, L. Du, C. Liu, X. Chen and J. J. Chruma, *ACS Omega*, 2021, **6**, 19291–19303.
182 F. Amaro, D. Silva, H. Reguengo, J. C. Oliveira, C. Quintas, N. Vale, J. Gonçalves and P. Fresco, *Int. J. Mol. Sci.*, 2020, **21**, 7968.
183 C. Lou, S. Yokoyama, S. Abdelhamed, I. Saiki and Y. Hayakawa, *Oncol. Lett.*, 2016, **12**, 295–300.
184 J. Meng, R. Su, L. Wang, B. Yuan and L. Li, *PeerJ*, 2021, **9**, e10692.
185 R. Zhang, G. Li, Q. Zhang, Q. Tang, J. Huang, C. Hu, Y. Liu, Q. Wang, W. Liu, N. Gao and S. Zhou, *Cell Death Dis.*, 2018, **9**, 598.
186 Z. C. Sun, C. F. Ma and X. L. Zhan, *J. Biochem. Mol. Toxicol.*, 2024, **38**, e23614.
187 F. Sommer, K. Obenaus and U. Engelmann, *Int. J. Impot. Res.*, 2001, **13**, 268–275.
188 A. T. Guay, R. F. Spark, J. Jacobson, F. T. Murray and M. E. Geisser, *Int. J. Impot. Res.*, 2002, **14**, 25–31.
189 M. Carro Juáreza and G. Rodríguez Manzo, *Behav. Brain Res.*, 2003, **141**, 43–50.
190 M. A. Saad, N. I. Eid, H. A. Abd El-Latif and H. M. Sayed, *Eur. J. Pharmacol.*, 2013, **700**, 127–133.
191 T. Nakazawa, K. Banba, K. Hata, Y. Nihei, A. Hoshikawa and K. Ohsawa, *Biol. Pharm. Bull.*, 2006, **29**, 1671–1677.
192 H. Takayama, Y. Iimura, M. Kitajima, N. Aimi, K. Konno, H. Inoue, M. Fujiwara, T. Mizuta, T. Yokota, S. Shigeta, K. Tokuhisa, Y. Hanasaki and K. Kimio, *Bioorg. Med. Chem. Lett.*, 1997, **7**, 3145–3148.
193 M. Dudek, J. Knutelska, M. Bednarski, L. Nowiński, M. Zygmunt, B. Mordyl, M. Głuch-Lutwin, G. Kazek, J. Sapa and K. Pytka, *PLoS One*, 2015, **10**, e0141327.
194 M. Kotańska, M. A. Marcinkowska, J. Knutelska, M. Zygmunt and J. Sapa, *J. Pre-Clin. Clin. Res.*, 2018, **12**, 67–71.

